JGR Atmospheres

Key Points:
- A total of 161 measured volatile organic compound emission factors is 26.1 ± 6.9 g kg^{-1}, 67% of which is from oxygenated species
- 76% of the total volatile organic compound emitted mass shows statistically significant dependence on modified combustion efficiency
- Mass fraction contributions of individual species to the total measured emissions have little variability in 24 western U.S. fires

Correspondence to:
L. Hu,
lu.hu@mso.umt.edu

Emissions of Trace Organic Gases From Western U.S. Wildfires Based on WE-CAN Aircraft Measurements

Wade Permar[1], Qian Wang[1,7], Vanessa Selimovic[1], Catherine Wielgasz[1], Robert J. Yokelson[1], Rebecca S. Hornbrook[2], Alan J. Hills[2], Eric C. Apel[2], I-Ting Ku[3], Yong Zhou[3], Barkley C. Sive[4], Amy P. Sullivan[3], Jeffrey L. Collett Jr[3], Teresa L. Campos[2], Brett B. Palm[5], Qiaoyun Peng[5], Joel A. Thornton[5], Lauren A. Garofalo[6], Delphine K. Farmer[6], Sonia M. Kreidenweis[6], Ezra J. T. Levin[3,8], Paul J. DeMott[3], Frank Flocke[2], Emily V. Fischer[3], and Lu Hu[1]

[1]Department of Chemistry and Biochemistry, University of Montana, Missoula, MT, USA, [2]Atmospheric Chemistry Observations & Modeling Laboratory, National Center for Atmospheric Research, Boulder, CO, USA, [3]Department of Atmospheric Science, Colorado State University, Fort Collins, CO, USA, [4]Air Resources Division, National Park Service, Denver, CO, USA, [5]Department of Atmospheric Sciences, University of Washington, Seattle, WA, USA, [6]Department of Chemistry, Colorado State University, Fort Collins, CO, USA, [7]Guizhou Provincial Key Laboratory of Geographic State Monitoring of Watershed, Guizhou Education University, Guiyang, China, [8]Handix Scientific, Boulder, CO, USA

Abstract We present emission measurements of volatile organic compounds (VOCs) for western U.S. wildland fires made on the NSF/NCAR C-130 research aircraft during the Western Wildfire Experiment for Cloud Chemistry, Aerosol Absorption, and Nitrogen (WE-CAN) field campaign in summer 2018. VOCs were measured with complementary instruments onboard the C-130, including a proton-transfer-reaction time-of-flight mass spectrometer (PTR-ToF-MS) and two gas chromatography (GC)-based methods. Agreement within combined instrument uncertainties (<60%) was observed for most co-measured VOCs. GC-based measurements speciated the isomeric contributions to selected PTR-ToF-MS ion masses and generally showed little fire-to-fire variation. We report emission ratios (ERs) and emission factors (EFs) for 161 VOCs measured in 31 near-fire smoke plume transects of 24 specific individual fires sampled in the afternoon when burning conditions are typically most active. Modified combustion efficiency (MCE) ranged from 0.85 to 0.94. The measured campaign-average total VOC EF was 26.1 ± 6.9 g kg^{-1}, approximately 67% of which is accounted for by oxygenated VOCs. The 10 most abundantly emitted species contributed more than half of the total measured VOC mass. We found that MCE alone explained nearly 70% of the observed variance for total measured VOC emissions ($r^2 = 0.67$) and >50% for 57 individual VOC EFs representing more than half the organic carbon mass. Finally, we found little fire-to-fire variability for the mass fraction contributions of individual species to the total measured VOC emissions, suggesting that a single speciation profile can describe VOC emissions for the wildfires in coniferous ecosystems sampled during WE-CAN.

1. Introduction

Wildland fires are a significant source of non-methane volatile organic compounds (VOCs) to the atmosphere, impacting downwind air quality, public health, and the formation of secondary pollutants such as ozone (O_3), and secondary organic aerosol (SOA) (Akagi et al., 2011; Crutzen & Andreae, 1990; Hatch et al., 2017; Koss et al., 2018; Liu et al., 2017). However, their global and regional emissions are highly uncertain, in part reflecting the scarcity of field measurements to constrain VOC emissions from biomass burning. As the size and intensity of wildfires in the western United States (U.S.) have increased due to historic forest management practices and climate change (Bowman et al., 2017; Jolly, 2015; Westerling, 2006, 2016), regional air quality is degrading relative to the rest of the country (McClure & Jaffe, 2018; O'Dell et al., 2019). These issues motivated comprehensive smoke characterization measurements from the National Science Foundation/National Center for Atmospheric Research (NSF/NCAR) C-130 research aircraft during the 2018 Western Wildfire Experiment for Cloud Chemistry, Aerosol Absorption, and Nitrogen (WE-CAN) field campaign (https://www.eol.ucar.edu/field_projects/we-can).

Biomass burning emission factors (EFs, g compound emitted per kg biomass burned) are a critical input to emissions inventories that are derived from vegetation/compound specific EFs and burned area, fuel

consumption per unit area, or fire radiative power (Kaiser et al., 2012; Larkin et al., 2014; van der Werf et al., 2017). Global and regional emission estimates for biomass burning are subjected to large uncertainties, often at a factor of 4–10, given the difficulty of estimating burned area and fuel consumption (Carter et al., 2020; Pan et al., 2020; Zhang et al., 2014) along with large fire-to-fire variability and generally limited observational constraints in many wildfire-prone regions, including the western U.S. (Jaffe et al., 2020; Prichard et al., 2020). For example, in a recent synthesis of field-measured temperate forest EFs, many species that are important in plume SOA and O_3 formation such as furans and terpenes (Coggon et al., 2019; Hatch et al., 2019), have only been reported in seven western U.S. wildfires (Andreae, 2019; Friedli et al., 2001; Liu et al., 2017). The large natural fire-to-fire variability of some commonly measured VOC emissions can be partially explained by modified combustion efficiency (MCE), which is a simple proxy of "flaming" and "smoldering" combustion processes readily calculated from observations of carbon monoxide (CO) and carbon dioxide (CO_2) (Akagi et al., 2013; Andreae & Merlet, 2001; Ferek et al., 1998; Guérette et al., 2018; Liu et al., 2017; Urbanski, 2014; Yokelson et al., 1999). However, the extent that MCE describes many of the rarely measured and reported compounds in wildfire smoke remains unknown.

To better constrain VOC and other air pollutant emissions from western U.S. fires, several recent large laboratory burn experimental studies have been conducted for representative fuels (Gilman et al., 2015; Hatch et al., 2017; Koss et al., 2018; Selimovic et al., 2018; Stockwell et al, 2014, 2015; Yokelson et al., 2013). Laboratory experiments attempt to simulate real-world burning conditions using fuels selected to replicate at least partially authentic fires, sometimes resulting in good agreement between field and laboratory measured EFs and emission ratios (ERs) of overlapping species (Akagi et al., 2013; Christian et al., 2003; Selimovic et al., 2018; Yokelson et al., 2008, 2013). However, laboratory burning experiments are imperfect proxies for the complexity of the dynamic burning processes, meteorological conditions, and varying fuels present in wildland fires. Meanwhile, many field emission measurements, either using ground-based or airborne-based platforms, are limited by how near a wildfire they can sample due to safety and logistical constraints. As chemical processes take place in the smoke plume within tens of minutes between emission and sampling by research aircraft (Akagi et al., 2012; Hobbs et al., 2003; Lindaas et al., 2021; Peng et al., 2020), field emission measurements reflect some removal of highly reactive species along with the formation of secondary products. Airborne measurements may also miss emissions from residual smoldering combustion (Bertschi et al., 2003), which tend to not be lofted into the main convective column of the plume, while near-field ground-based measurements reflect the opposite problem as they are often unable to sample portions of the smoke most impacted by flaming emissions (Akagi et al., 2013; Ottmar, 2014; Prichard et al., 2020; Yokelson et al., 2013). Additionally, laboratory studies can allow for a large suite of analytical instrumentation to sample smoke within meters of a fire, from ignition to extinction. Field measurements are often limited by instrument payload and include emissions from a variety of burning conditions. Consequently, to most accurately characterize wildfire emissions, insights gained from laboratory studies are useful for interpreting field measurements (Selimovic et al., 2019).

Hundreds, if not thousands, of VOCs are known to be present in biomass burning smoke (Bruns et al., 2017; Hatch et al., 2017; Koss et al., 2018; Müller et al., 2016; Stockwell et al., 2015). Characterization of these VOCs remains a challenge though, with no single technique best suited to measure such a large variety of compounds, particularly at the temporal resolution needed for aircraft sampling. Chemical ionization mass spectrometry (CIMS), such as proton-transfer-reaction time-of-flight mass spectrometry (PTR-ToF-MS), is capable of measuring hundreds of VOCs at <1 s, but does not provide isomer speciation without co-deployed auxiliary techniques. Gas chromatography (GC)-based systems are highly complementary to CIMS instruments, providing speciated VOC measurements with low ppt detection limits at lower temporal resolution. During the recent Fire Influence on Regional to Global Environments Missoula Fire Lab experiment (FIREX-MFL, https://www.esrl.noaa.gov/csl/projects/firex/firelab), Koss et al. (2018) identified the VOC contributors to more than 150 ions detected by PTR-ToF-MS (~90% of the total detected VOC mass) through a combination of approaches including gas chromatography pre-separation, two chemical ionization methods, literature review, and time-series correlation. Additionally, Sekimoto et al. (2017) showed that sensitivities for many VOCs without direct calibrations in PTR-ToF-MS can be calculated to within an uncertainty of ± 50% using readily available molecular properties such as polarizability, dipole moment, and functionality.

In this study, we utilize data from the co-deployed GC-based Trace Organic Gas Analyzer (TOGA) and the Advanced Whole Air Sampler (AWAS), while building extensively off previous identification, calibration, and validation efforts for PTR-ToF-MS, to report emissions for 161 individual VOCs and ion masses, plus five non-VOCs (CO_2, CO, CH_4, BC, and OC) for western U.S. wildfires. This represents nearly double the number of VOCs reported for temperate forests in the most recent synthesis study by Andreae (2019), offering more complete measurements of the total VOC emissions from wildfires. To the best of our knowledge, it is also the first time many of the VOCs recently identified in laboratory studies have been measured in the field under real-world fire conditions. Additionally, the unprecedented large number of wildfires sampled during WE-CAN doubles the number of western U.S. airborne samples for near-field fire emissions, allowing us to explore the variability of VOC emissions and how they are related to combustion processes.

2. Methods

2.1. WE-CAN Field Campaign

The WE-CAN field campaign was based on Boise, ID, from July 24 to August 31 and Broomfield, CO from September 1 to 13, 2018. Nineteen flights were conducted by the NSF/NCAR C-130 research aircraft approximately every 1–3 days and sampled smoke from fires across seven western states (Juncosa Calahorrano et al., 2021; Lindaas et al., 2021). Smoke plumes were typically sampled between 14:00 and 19:00 local time when burning conditions were most active. Most sampled smoke plumes were emanating from wildfires located in mixed coniferous ecosystems primarily dominated by pine, fir, and spruce trees (http://catalog.eol.ucar.edu/we-can/tools/fccs). Sampling of fresh emissions was done by flying perpendicular transects through each smoke plume as near to the source as was allowed by safety and logistical constraints. Emissions were assessed using transects that proceeded as follows. The C-130 entered into each plume after sampling background air as determined by real-time CO observations in flight and continued through the plume until the CO mixing ratios reached regional background levels (generally 75–175 ppb), ideally similar to the mixing ratios observed before entering the plume. During WE-CAN, the C-130 also sampled smoke plumes in a pseudo-Lagrangian fashion to characterize smoke evolution (Akagi et al., 2012); other portions of the flights were devoted to sampling cloud-smoke mixtures and aged regional smoke plumes in specific locations. In this analysis, we focus on the WE-CAN VOC EFs while emission information for NH_3, NO_x, and other reactive nitrogen species can be found in Lindaas et al. (2021) and Peng et al. (2020), and ERs for organic aerosol are available in Garofalo et al. (2019).

2.2. Proton-Transfer-Reaction Time-Of-Flight Mass Spectrometer

We deployed the University of Montana PTR-ToF-MS (Model 4000, Ionicon Analytik) aboard the NSF/NCAR C-130 during WE-CAN. This represents only the second time a PTR-ToF-MS had been used to measure smoke from an aircraft and the first where smoke sampling was the primary mission objective. The PTR-ToF-MS is custom-built into a standard NSF/NCAR HIAPER Gulfstream-V (GV) rack with the mass spectrometer separately vibration dampened. Drift tube conditions were maintained at 3.00 mbar, 810 V, and 60°C, resulting in an E/N of 130 Td for the duration of the campaign. Ions m/z from 15 to 400 were measured at 2 or 5 Hz frequency with a mass resolution of 2,250 $m/\Delta m$ at m/z 33.033 and 4,000 $m/\Delta m$ at m/z 330.842, where Δm is the full width at half mass for an ion peak of mass m.

The PTR-ToF-MS inlet was positioned below the instrument rack, mid-cabin underneath the aircraft. Ambient air was drawn into the cabin at 10–15 lpm, dependent on altitude, via a heated (60°C) NCAR HIAPER Modular Inlet (HIMIL) attached to a downstream pump (KNF Neuberger Inc.). From the HIMIL to the instrument rack, sampled air traveled a distance of ~3 m through 3.175 mm I.D. PFA tubing maintained at ~55°C by a self-regulating heat cable. At the rack, the sample stream was subsampled by the PTR-ToF-MS through ~100 cm of 1.588 mm O.D. PEEK tubing maintained at 60°C. The residence time from outside the plane to the drift tube was less than 2 s. A detailed schematic of our instrument inlet and sampling setup is provided in Figure S1.

For a typical research flight, the PTR-ToF-MS was powered on and allowed to pump down starting 3 h before takeoff. Instrument background was checked approximately every hour by measuring VOC-free air generated from a heated catalytic converter (375°C, platinum bead, 1% wt. Pt, Sigma Aldrich) for 3 min. Real-time mass calibrations were performed every 5 s using an internal 1,3-diiodobenzene ($C_6H_4I_2$) reference standard added directly to the drift tube from an adjacent heated permeation device.

Mass spectra were analyzed using Ionicon's PTR-MS Viewer software (version 3.2.8.0, Ionicon Analytik). Postflight mass calibrations were done to further refine the real-time mass calibration using 5 ion peaks: m/z 18.0338 [NH_3H^+], 29.9971 [NO^+], 59.0491 [$C_3H_6OH^+$], 203.943 [$C_6H_4IH^+$], and 330.848 [$C_6H_4I_2H^+$]. Chemical formulas for each ion mass were assigned using a peak list native to the software as well as derived from the growing PTR-ToF-MS literature (Koss et al., 2018; Pagonis et al., 2019). A high-resolution peak fitting algorithm was then manually adjusted for individual peak shapes and PTR-MS Viewer calculated ion counts for each peak, performing a baseline correction, and correcting for mass discrimination in the time-of-flight following common standard PTR-ToF-MS data analysis procedures (Yuan et al., 2017).

Mass transmission corrected raw instrument signals were exported for post-processing in R (R Core Team, 2019), using the open-source software RStudio with the dplyr and ggplot2 packages (RStudio Team, 2020; Wickham, 2016; Wickham et al., 2019). Ion masses were first background corrected by subtracting the linearly interpolated instrument background measured in-flight. Ion counts were then normalized to the primary ion signal and a humidity correction factor was applied for those VOCs which were calibrated by the gas standard (de Gouw et al., 2003). PTR-ToF-MS data in normalized counts per second (ncps) were averaged to 1 Hz and converted to mixing ratios as described in Section 2.2.2 for all subsequent analyses.

2.2.1. Identification and Speciation of PTR-ToF-MS Ion Masses

Overlapping speciated VOC measurements available on the C-130 during WE-CAN (Section 3) allow us to identify and assign isomeric fractional contributions to four PTR-ToF-MS ions masses (Table S1): m/z 59.049, m/z 71.049, m/z 107.086, and m/z 137.132. For the remaining ions, we applied available isomeric contributions measured during the FIREX-MFL study, which burned similar western U.S. fuel types and speciated PTR-ToF-MS ion peaks for an instrument with a similar mass resolving power to the one deployed during WE-CAN (Koss et al., 2018). Although the actual isomeric contributions may differ, especially for relatively reactive species, the consistent treatment of PTR-ToF-MS measurements between FIREX-MFL and WE-CAN allows for a more direct comparison of the EFs determined in the laboratory to our field observations (Section 6). The overall measurement uncertainty caused by assumptions in isomeric contributions are mostly governed by the instrument sensitivities for all isomers which differ by less than 50% at any given ion mass, indicating that the impact on mixing ratio is within the error of the calculated sensitivities (see Section 2.2.2)

During WE-CAN, we quantified 125 out of 154 identified ions (excluding ammonia, NH_3, and nitrous acid, HONO) reported during FIREX-MFL (Koss et al., 2018). The remaining 29 ions accounted for less than 2% of the FIREX-MFL PTR-ToF-MS total measured VOC mass (sum of VOC EFs). Additional quantification in the laboratory resulted largely from Fourier-transform infrared spectroscopy (FTIR) co-measured data for NH_3 and HONO (Selimovic et al., 2018) and the fact that laboratory burning experiments measure emissions at ~10 times higher sample concentrations than field observations (Stockwell et al., 2014). In later sections, we discuss if the identification and speciation of ion masses from laboratory studies are represented in the field as constrained by the limited co-measured VOCs onboard the C-130 aircraft (Section 3), and describe how the difference of plume aging between laboratory and field measurements may affect EFs (Section 6).

2.2.2. Calibration

For each flight, we calibrated the instrument three times: 10 min before takeoff, in-flight when in transit to/from a fire, and immediately after landing. Instrument calibrations were carried out by the dynamic dilution and subsequent addition of 25 distinct VOCs from two compressed gas standard cylinders (stated accuracy 5% at ~1 ppmv; Apel-Riemer Environmental Inc.; species listed in Figure S2) to the VOC-free air described above. The standard gas cylinders were filled in June 2017 and were re-analyzed for selected VOCs before and after the WE-CAN campaign with the permeation device described below. Calibrations

were carried out in the range of 1–10 ppb. Typical r^2 values for the 4-point calibration curve of all species were greater than 0.99 with average residual standard errors less than 10% (in almost all cases <3%). The standard error (95% confidence interval) of sensitivities for all calibrated VOCs was found to be <9% during WE-CAN, thus the campaign averaged sensitivities were applied to all flights. The overall uncertainty for gas standard calibrated species is <15%, which is based on the quadrature addition of the individual errors including mass flow controllers, standard accuracy, peak fitting, and calibration.

Additionally, we calibrated formaldehyde (HCHO) post WE-CAN using a gas standard (accuracy 5% at 420 ppbv reanalyzed by FTIR in October 2019). We quantified the humidity dependent sensitivity by varying the water vapor in the zero air to the range observed during WE-CAN (i.e., $[m/z\ 39]/[m/z\ 21]$, an internal humidity proxy, spanning 0%–2%) (Vlasenko et al., 2010; Warneke et al., 2011), and accounted for a possible sensitivity drift since WE-CAN based on other gas standard calibrations. The formaldehyde measurement uncertainty is estimated to be 40%, mostly contributed by instrument sensitivity drift since WE-CAN.

We also calibrated acetic acid (CH_3COOH) and formic acid (HCOOH) before and after the campaign using a custom built permeation system (Baasandorj et al., 2015; Haase et al., 2012; Veres et al., 2010). Here, a constant flow of 20 sccm of ultrapure zero air was passed over a PFA permeation tube (fabricated in-house), which was maintained at a constant temperature. The VOC mixing ratio from the permeation source was stoichiometrically determined by converting to CO_2 via passing through a heated catalyst (400°C, platinum bead, 1% wt. Pt, Sigma Aldrich) and subsequently measuring enhancement by a CO_2 detector (LI-840A, LI-COR Inc). Analytes were then added into the PTR-ToF-MS via the above dynamic dilution calibration. The performance of the permeation system was verified by both certified permeation tubes and the multi-component gas standards. The uncertainty in the permeation calibrations is generally less than 30%, contributed mostly by the LI-COR.

For the remaining ∼180 identified VOCs that are not directly calibrated, we estimated their instrument sensitivities using the method developed by Sekimoto et al. (2017). Briefly, molecular dipole moments and polarizability for each species are used to calculate a proton capture coefficient, k_{cap}, for the reaction with H_3O^+. k_{cap} was shown to be linearly correlated to sensitivity for most VOCs:

$$Sensitivity_{calculated,i} = a \times k_{cap,i} \tag{1}$$

where the coefficient a is experimentally determined from calibrated VOCs and their k_{cap} ($a = 5.00 \times 10^9$ for the instrument setting in WE-CAN). Chemical properties used here, including functional groups, polarizabilities, and dipole moments, are from the compiled PTR-ToF-MS Library (www.tinyurl.com/PTRLibrary; Pagonis et al., 2019).

The overall uncertainty for this method is estimated to be 50% for most species and may be higher for select groups of VOCs (Sekimoto et al., 2017). The calculated and measured sensitivity for 26 directly calibrated VOCs are compared in Figure S2, showing agreement within the stated uncertainty. Sensitivity estimates are further verified for co-measured VOCs onboard the C-130 in Section 4.

Average sensitivities for each ion mass were subsequently determined using the weighted sensitivity of the known isomers following:

$$sensitivity_{average} = \left(\sum \frac{contribution_i}{sensitivity_i} \right)^{-1} \tag{2}$$

where $contribution_i$ is the isomeric contribution of VOC isomers to an ion mass (Section 2.2.1) and $sensitivity_i$ is the corresponding instrument calibration factor either from direct calibrations using gas standards or calculated using molecular properties. The overall uncertainty is then estimated by adding in quadrature errors from involved sensitivities weighted by isomeric contributions. Table S1 lists the sensitivities for 180 VOCs, along with their uncertainties, isomeric contributions to each mass, and calibration methods.

2.3. TOGA, AWAS, I⁻ CIMS, and Other Supporting Instrumentation

In addition to PTR-ToF-MS, we report VOCs measured by the Trace Organic Gas Analyzer (TOGA) (Apel et al, 2003, 2010, 2015; Hornbrook et al., 2011), Advanced Whole Air Sampler (AWAS) (Andrews et al., 2016), and iodide (I⁻) adduct high-resolution time-of-flight chemical-ionization mass spectrometer (I⁻ CIMS) (Lee et al., 2014; Palm et al., 2019; Peng et al., 2020). The TOGA and AWAS measurements greatly extend the emission analysis here to include many species not detected by PTR-ToF-MS, while also adding isomer contributions for several ion masses. During WE-CAN, TOGA sampled ambient air for 28–33 s to a liquid nitrogen-cooled cryogenic preconcentrator, which was then analyzed for 72 VOCs every 100–105 s via a gas chromatography-mass spectrometer (GC-MS). The collection of AWAS canister samples was manually initiated based on inflight measured CO mixing ratios targeting both edges and the center of a plume. Typically, 1–3 canister samples were collected per emission transect in addition to background samples collected either just outside a smoke plume or behind the fire. Each canister was filled for 3–7 s and analyzed for 58 individual VOCs (C_1–C_{10} hydrocarbons, C_1–C_5 alkyl nitrates, and oxygenated VOCs) using a five-channel gas chromatography system equipped with three flame ionization detectors, one electron capture detector, and one mass spectrometer (Benedict et al, 2019, 2020; Russo et al., 2010; Zhou et al., 2010). Measurement uncertainties for TOGA and AWAS vary by compound but are typically between 15% and 50% (TOGA) and <10% (AWAS). We also report HCOOH measured by I⁻ CIMS because of its high sensitivity. I⁻ CIMS HCOOH calibration uncertainty is 30% and was measured at 2 Hz (Palm et al., 2019; Peng et al., 2020).

CO, measured at 1 Hz (accuracy 1 ppb, 2σ) by quantum cascade laser spectrometry (CS-108 miniQCL, Aerodyne Inc.) was used for all analyses except for fires sampled on August 13, 2018 (RF10), where we used a cavity ring down spectrometer (G2401-m WS-CRD, Picarro) which also measured CO_2 (accuracy 100 ppb, 2σ) and CH_4 (accuracy 3 ppb, 2σ) at 1.3 Hz for the duration of the campaign.

Black carbon (mass equivalent diameter ∼90–500 nm) was measured by a single particle soot photometer (SP2) (Liu et al., 2017; Schwarz et al., 2008) and averaged to a 10 s sampling frequency. When in a plume, the SP2 sample was diluted with HEPA-filtered ambient air to prevent signal saturation (Garofalo et al., 2019) and has an uncertainty of 40% when on the dilution system. Organic carbon (OC) was determined by high-resolution aerosol mass spectrometry (HR-AMS; Aerodyne Inc.). HR-AMS operation during WE-CAN is described in Garofalo et al. (2019) and OA:OC ratios were determined via improved ambient elemental analysis for AMS (Canagaratna et al., 2015). For the analysis shown here, OC was calculated in the nascent HR-AMS time resolution (5 s) from the simultaneously measured OA mass concentration and OA:OC ratio. When OA:OC was unavailable due to OA being below the instrument detection limit during background sampling, we used the average background OA:OC ratio of 2.02. HR-AMS measured OA with vacuum aerodynamic diameter of ∼70–1,000 nm and uncertainty of 35%, while the OA:OC uncertainty is 8%. The average OA:OC ratio for the emissions transects used in this study is 1.73.

2.4. Co-Measured VOCs and Data Reduction

Of the 161 VOC species reported in this study, 34 were co-measured by PTR-ToF-MS, TOGA, and/or AWAS. For overlapping VOC measurements, we used similar criteria as in Yokelson et al. (2013) to determine which measurement to report. Selection criteria are hierarchically described below.

(1) Species that PTR-ToF-MS is known to have difficulty measuring because of low sensitivities or interfering fragments were removed from the analysis and the appropriate TOGA or AWAS measurement was used instead. These include hydrogen cyanide (HCN), ethane (C_2H_6), ethanol (C_2H_5OH), and dimethyl sulfide (DMS, $(CH_3)_2S$). Similarly, we removed PTR-ToF-MS measured isoprene (C_5H_8) due to possible fragment interference as discussed in Section 4.

(2) When selecting between species co-measured by TOGA and AWAS, we retained the measurement reporting the most isomers for a given chemical formula. When the number of observed isomers was equal, we report the measurement with the greater campaign average ER for that chemical formula to account for potential unidentified species.

(3) VOCs directly calibrated by the PTR-ToF-MS (Figure S2) were selected over TOGA or AWAS measurements to preserve the high time resolution of the measurement. It also helps minimize possible errors from (1) background correcting discrete samples, (2) misalignment of the discrete data to the

high-frequency CO measurements, and (3) the potential for discrete samples only capturing part of a plume. For VOCs with known isomers or fragments in PTR-ToF-MS, we also report the TOGA or AWAS measurement as described in criteria 2. However, to prevent double counting, additional speci-ated information was not used in EF mass balance or total emitted VOC calculations.

For example, PTR-ToF-MS measures the total of methyl vinyl ketone (MVK), methacrolein (MACR), and 2-butenal at m/z 71.049 ($C_4H_6OH^+$; Table S1). TOGA and AWAS both report individual MVK and MACR, with TOGA also measuring 2-butenal. For the EF calculations here, we used the PTR-ToF-MS measurement for m/z 71.049. Additionally, we included the TOGA MVK, MACR, and 2-butenal measurements in Table 2 to provide more detailed speciation, and because TOGA observed more isomers than AWAS. When totaling carbon, EFs, or ERs, only the PTR-ToF-MS measurement was used.

(4) For VOCs with calculated sensitivities, we used the PTR-ToF-MS measurement when campaign-average emission transect mixing ratios agree within 50% of the sum of TOGA or AWAS isomers for that mass. Additionally, if the PTR-ToF-MS does not agree within 50% but there are known isomers not reported by TOGA or AWAS, we again report the PTR-ToF-MS measurement with TOGA or AWAS speciation as described in criteria 3. For the remaining species where the PTR-ToF-MS does not agree within 50%, we again report the appropriate TOGA or AWAS measurement following criteria 2.

2.5. Calculations of Emission Factors, Emission Ratios, and Modified Combustion Efficiency

We calculated WE-CAN EFs and ERs for 31 emission transects of 13 wildfires and 1 prescribed burn. Plume transects were chosen for inclusion based on the criteria of being from well-defined smoke plumes tracea-ble to a single emission source, being the nearest transects to said source, and having physical age less than 130 min as calculated by wind speeds measured aboard the C-130 and fire locations reported by the U.S. For-est Service (http://catalog.eol.ucar.edu/we-can/tools/fuels). The latter criterion was chosen to reflect aging times in similar studies (Liu et al., 2017) and maximize the number of plume transects available to improve statistics. Recent studies have shown that rapid chemistry occurs within minutes after emission (Akagi et al., 2012; Hobbs et al., 2003; Lindaas et al., 2021; Peng et al., 2020); later we discuss how this may affect the EFs for some very reactive VOCs that we report here. For repeated sampling, we aggregate those plume transects which were performed in succession for the same fire within 30 min and treat those that are more than 30 min apart as "unique fires." This results in 24 fires used in the emission analysis here (denoted a, b, c, etc., Tables 1 and S4).

Excess mixing ratios (Δ) for high rate measurements were determined per transect by subtracting the linearly interpolated background between air measured immediately outside both edges of the plume transect as determined by CO and acetonitrile levels. For lower rate measurements by TOGA and AWAS, Δ was calculated using the average background of the samples taken nearest one or both edges of a plume transect.

ERs were calculated by integrating the background-corrected in-plume measurements and dividing by the plume-integrated excess CO mixing ratio (averaged over each measurement's sampling time). We note that ERs here are calculated by integrating PTR-ToF-MS and CO real-time plume measurements, rather than using the slope of the least squares regression of ΔVOC versus ΔCO, to minimize potential biasing of ERs by the center or edge of plume measurements and limit potential error caused by discrepancies in instrument timing (Garofalo et al., 2019).

EFs were calculated using the carbon mass balance method, assuming all burnt carbon is volatilized and detected following (Yokelson et al., 1999):

$$EF_{VOC} = F_c \times 1000 \left(\frac{g}{kg} \right) \times \frac{MW_{VOC}}{12} \times \frac{\frac{\Delta VOC}{\Delta CO}}{\sum_{i=1}^{n} \left(NC_i \times \frac{\Delta VOC_i}{\Delta CO} \right)} \tag{3}$$

Table 1
Details of Fires Sampled During the WE-CAN Field Campaign Used in This Work

Fire Name[a]	Date (2018)	Flight	State	Num. Passes[b]	Latitude	Longitude	Distance Sampled Downwind (km)	Physical Age (minutes)	Burned Area (ha)[c]
Carr (a, b)	July 26	RF02	CA	1, 1	40.63°	-122.52°	32.8–33.6	64–106	92,939
Taylor Creek	July 30	RF03	OR	2	42.47°	-123.69°	11.5–13.7	22–27	21,383
Sharps (a, b)	July 31	RF04	ID	2, 1	43.59°	-114.16°	18.4–19.9	50–85	26,209
Rabbit Foot (a, b, c)	August 3	RF06	ID	1	44.86°	-114.27°	11.2–29.8	22–78	14,570
	August 13	RF10		1					
	August 15	RF11		5					
Donnell (a, b)	August 6	RF07	CA	1, 2	38.36°	-119.88°	35.7–45.5	66–106	14,751
Bear Trap (a, b)	August 9	RF09	UT	1, 1	39.29°	-109.87°	11.5–30.6	30–74	4,955
Dollar Ridge	August 9	RF09	UT	1	40.14°	-110.88°	29.6	118	27,870
Monument	August 13	RF10	MT	1	45.00°	-111.82°	15.2	27	2,676
Wigwam	August 13	RF10	MT	1	45.14°	-111.89°	14.4	18	1,654
Goldstone (a, b)	August 13	RF10	MT/ID	1	45.11°	-113.56°	13.8–51.9	19–121	3,787
	August 15	RF11		1					
Beaver Creek (a, b)	August 15	RF11	MT	1, 1	45.94°	-113.51°	27.3–56.2	57–127	845
Mendocino Complex	August 20	RF13	CA	1	39.43°	-122.84°	57.1	120	185,804
Red Feather Prescribed Burn (a, b)	September 10	RF18	CO	1, 1	40.85°	-105.58°	3.5–4.8	17–17	1,759
Silver Creek (a, b)	September 13	RF19	CO	1, 1	40.23°	-106.60°	24.7–27.3	23–28	8,142

[a]Letters in parentheses denote smoke plumes sampled more than 30 min apart, where each is treated separately in emission factor calculations (Section 2.5). [b]Number of emission transects per fire as denoted by a, b, or c. Emission transect times can be found in Table S4. [c]Total area burned by the fire before being extinguished, sourced from https://www.fireweatheravalanche.org.

where F_c is the mass fraction of carbon in the fuel (0.457), MW_{VOC} is the molecular mass of a given VOC, 12 is the atomic mass of carbon, $\frac{\Delta VOC}{\Delta CO}$ is the ER of VOC to CO in ppb ppb^{-1}, NC_i is the number of carbon atoms in VOC$_i$, and the sum is over all carbon containing species including 161 ions and individual VOCs measured by PTR-ToF-MS, AWAS, TOGA, and I$^-$ CIMS, along with organic carbon (OC), black carbon (BC), CO, CO$_2$, and CH$_4$. We use 45.7% for the percent carbon of western U.S. fuels (Santín et al., 2015) as justified by Liu et al. (2017) for computing EFs (Section 6).

Additionally, to explore the dependence of EFs on the combustion efficiency (Section 7), we calculated the MCE for each emission transect using the plume integrated excess CO and CO$_2$ mixing ratios:

$$MCE = \frac{\Delta CO_2}{\Delta CO_2 + \Delta CO} \tag{4}$$

3. Inferred Isomeric Contribution to PTR-ToF-MS Ion Masses in Fire Smoke

The TOGA instrument aboard the C-130 during WE-CAN provides sufficient constraints to quantify the isomeric fractional contributions for four PTR-ToF-MS ion masses using 12 TOGA speciated VOCs measured in 20 emission transects (Figure 1; Table S1). Such isomeric information fills a gap in PTR-ToF-MS measurements and is rarely available due to limited co-deployed instruments, especially in fire smoke with complex mixtures of VOCs (Section 2.2.2). Koss et al. (2018) found that the isomeric fractional contributions tended to be similar across different fire burns and fuel types during FIREX-MFL. Here we use TOGA measurements to constrain the isomeric contribution to PTR-ToF-MS ion masses and examine consistency with laboratory studies and their natural variability in wildfires.
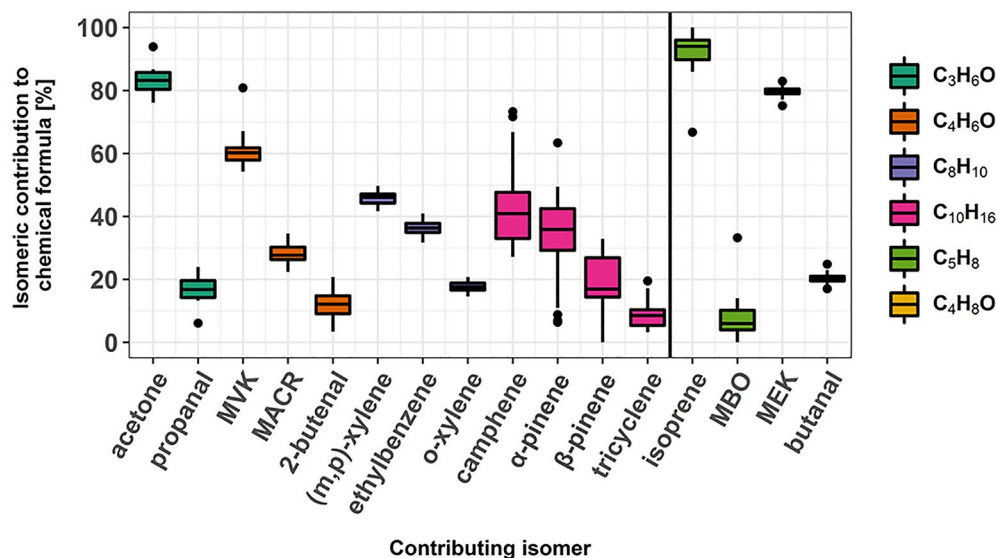
Figure 1. Individual isomer contributions to PTR-ToF-MS ions as measured by TOGA from 20 emission transects during WE-CAN. Box and whisker plots (boxes: 25th and 75th percentiles, horizontal line: median, whiskers: 1.5 × the inter quartile range, points: >1.5 × inter quartile range) are grouped by color corresponding to a single chemical formula. VOCs to the left of the vertical line were used to speciate four PTR-ToF-MS ion masses in this study. Isoprene and MBO are not isomers but are included due to the potential for MBO to contribute a significant interfering fragment to m/z 69.070 in coniferous forests (Karl et al., 2012). MEK and butanal, m/z 73.065, are not used for speciation because ~14% of the signal may be from 2-methylpropanal (Koss et al., 2018), which was not measured aboard the C-130. Note that β-pinene also includes myrcene.

Figure 1 and Table S1 shows the isomeric contributions for m/z 59.049 (acetone and propanal), m/z 71.049 (MVK, MACR, and 2-butenal), m/z 107.086 (m-, p-, o-xylenes and ethylbenzene), and m/z 137.132 (monoterpenes). Two additional ion masses at m/z 69.070 and m/z 73.065 are also shown. Both the WE-CAN field and FIREX-MFL laboratory measurements indicate MVK is the largest contributor at m/z 71.049 (60 ± 9% (1σ) WE-CAN, 48% FIREX-MFL) and acetone at m/z 59.049 (83 ± 6% WE-CAN, 100% FIREX-MFL). The WE-CAN isomeric contributions of m/z 107.086 differ the most from FIREX-MFL, but still show some consistency: (m, p)-xylenes are the major contributor (46 ± 5% WE-CAN, 68% FIREX-MFL) followed by ethylbenzene (36 ± 6% WE-CAN, 10% FIREX-MFL) and o-xylene (18 ± 10% WE-CAN, 23% FIREX-MFL).

At m/z 137.132, four monoterpenes (camphene, α-pinene, β-pinene + myrcene, and tricylene) were measured by TOGA on the C-130. We approximately speciate m/z 137.132 using WE-CAN measurements but note that laboratory burn studies have recently identified more than 30 monoterpene isomers. Among them, the most dominant compounds vary by fuel type, generally including β-pinene, 3-carene, limonene, α-pinene, and camphene (Hatch et al., 2017, 2019). Though we are likely missing key information to fully assign isomeric fractions for monoterpenes measured by PTR-ToF-MS, we do not expect additional speciation to change the total PTR-ToF-MS monoterpene measurement since the calculated sensitivities for additional isomers would be the same due to their identical chemical formula and functionalities (Sekimoto et al., 2017).

We do not attempt to fully speciate m/z 73.065 because only methyl ethyl ketone (MEK) and butanal were measured by TOGA during WE-CAN, while Koss et al. (2018) suggest a nonnegligible amount of 2-methylpropanal (14%) may be present at this mass in the laboratory burn experiment. Nonetheless, both studies agree that MEK is the dominant species at m/z 73.065 contributing 80 ± 2% during WE-CAN and 85% during FIREX-MFL.

PTR-ToF-MS measured isoprene (m/z 69.070) is known to have interfering fragments from 2-methyl-3-buten-2-ol (MBO), which is potentially emitted in more abundance biogenically than isoprene in western U.S. coniferous forests (Karl et al., 2012). Figure 1 shows the fractional contribution of isoprene and MBO for the hypothetical case of all MBO fragmenting and being detected at m/z 69.070 (i.e., their ratio to the

sum of isoprene and MBO). In this scenario m/z 69.070 would be 93 ± 9% isoprene, suggesting that in western U.S. wildfire emissions, MBO may not be a significant interfering fragment.

We find isomeric fractional contributions vary relatively little from fire-to-fire during WE-CAN, with standard deviations across 20 emission transects less than 10% for half of the isomers shown in Figure 1. Monoterpenes (31%–60%) and MBO (96%) fractional contribution standard deviations vary the most between emission transects, likely reflecting changing background levels in the lofted air above the forests. Though these above six ion masses constrained by TOGA are a small sample of all isomeric fractional information needed for PTR-ToF-MS measurements, the small observed fire-to-fire variation hints that the ratios of isomers measured in the laboratory are comparable to similar fuels measured in the field.

4. Instrument Intercomparison

Here, we compare the co-deployed PTR-ToF-MS, TOGA, and AWAS VOC observations. Though at lower sampling frequencies, both TOGA and AWAS GC-based measurements observe many VOCs not detected by PTR-ToF-MS while providing additional analytical separation power. We focus on the 24 "unique fire" emission transects and assess the implications of instrument uncertainties for measuring wildfire emissions. Whenever possible, multiple isomers measured by each method are summed together for comparison.

Figure 2 summarizes intercomparison results from the reduced major axis regression between PTR-ToF-MS and the two GC-based instruments. Most of the VOCs directly calibrated by PTR-ToF-MS, with only a single known isomer, and little interference due to fragments (formaldehyde, methanol, acetonitrile, acetaldehyde,
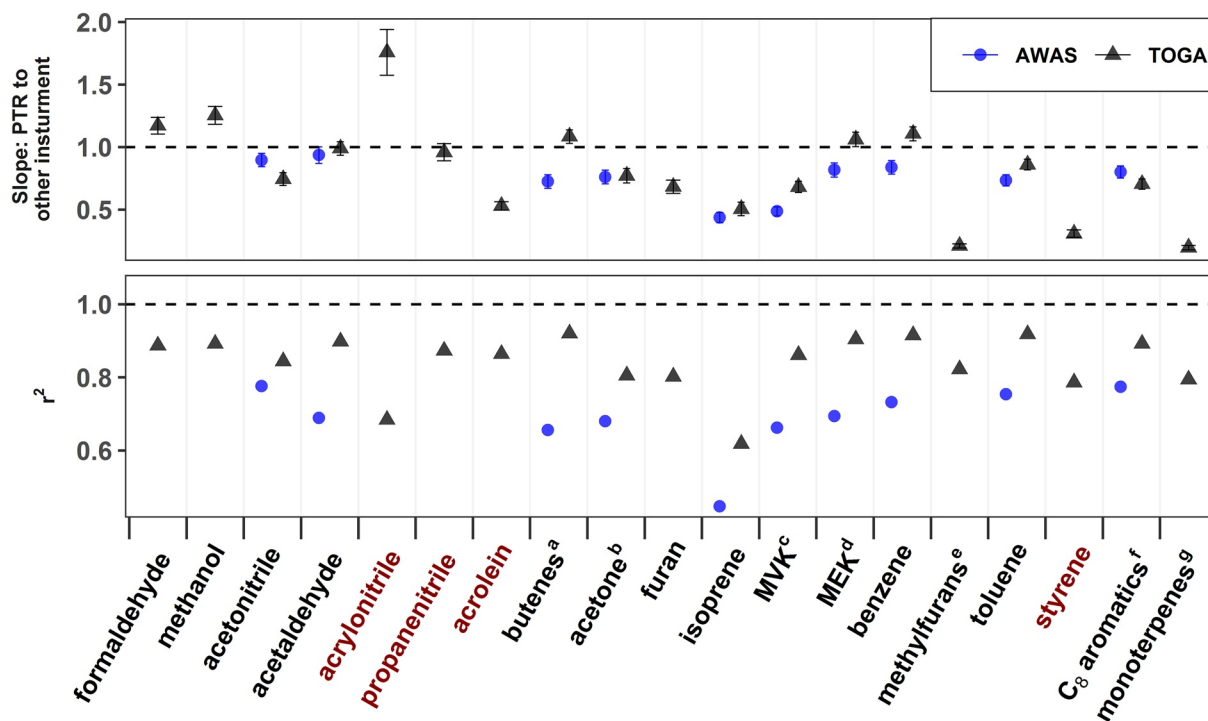

Figure 2. Slope and correlation coefficients (r^2) of the reduced major axis regression of PTR-ToF-MS versus TOGA (blue circles) and AWAS (black triangles) mixing ratios for all available emission transect measurements used in this study (~34 TOGA samples and ~40 AWAS samples). Slopes <1 mean that PTR-ToF-MS measured values are higher than TOGA or AWAS values. Error bars show the standard error of the slope, often too small to be discernible behind the points. VOCs in red have calculated PTR-ToF-MS calibration factors (Sekimoto et al., 2017), while VOCs in black have at least one directly calibrated isomer. Names for the most abundant VOC for each chemical formula are shown while superscripts denote VOCs where multiple isomers measured by TOGA or AWAS are summed together for comparison to the PTR-ToF-MS measurement. [a]TOGA: isobutene, 1-butene; AWAS: 1-butene, cis-2-butene, and trans-2-butene. [b]TOGA: acetone and propanal; AWAS: acetone. [c]TOGA: MVK, MACR, 2-butenal; AWAS: MVK and MACR. [d]TOGA: MEK and butanal; AWAS: MEK. [e]TOGA: 2-methylfuran and 3-methylfuran. [f]TOGA: (m,p)-xylenes, ethylbenzene, and o-xylene; AWAS: (m,p)-xylenes, ethylbenzene, and o-xylene. [g]TOGA: camphene, α-pinene, β-pinene + myrcene, and tricylene.

benzene, and toluene) agree within combined measurement uncertainties with the GC instruments, typically <30%. PTR-ToF-MS calibrated masses with identified contributing isomers or interfering fragments including butenes, acetone/propanal, MVK/MACR/2-butenal, MEK/butanal/2-methylpropanal, ethylbenzene/(*m,p*)- and *o*-xylenes (*m/z* 57.070, 59.049, 71.049, 73.064, and 107.085, respectively) also agree within ±30%.

Notable disagreement is found for five ion masses. PTR-ToF-MS measured isoprene is ~2 times higher than either TOGA or AWAS during smoke sampling. However, when sampling over forested regions with relatively little smoke influence, TOGA, AWAS, and PTR-ToF-MS isoprene agree within the combined uncertainty (not shown). Additionally, the PTR-ToF-MS isoprene shows poor correlation with the two GC instruments while in smoke ($r^2 = 0.43$), which suggests further fragment interference while in a plume than the 37% that we removed based on FIREX-MFL results (Koss et al., 2018). As mentioned in Section 3, TOGA typically measured little MBO relative to isoprene in WE-CAN emission transects, thus its fragments are not likely to be the major contributor. Additionally, cyclohexane fragments could play a role (Gueneron et al., 2015; Yuan et al., 2014), though their contribution in wildfire smoke is likely small as TOGA measured isoprene ERs were nearly 12 times higher than cyclohexane measured by AWAS during WE-CAN. Subsequently, the source of any additional fragments in fire smoke is currently unknown.

Total monoterpene abundance measured by PTR-ToF-MS is ~5 times higher than the sum of camphene, α-pinene, β-pinene/myrcene, and tricyclene measured by TOGA. This is likely due to a combination of factors. First, over 30 different monoterpene isomers have been detected in smoke, with the dominant isomers being highly variable between fuels (Hatch et al., 2017, 2019), while only four monoterpene isomers were reported by TOGA during WE-CAN (Figure 1). It is likely a large proportion of speciated monoterpenes were not measured here (Section 3). Second, the PTR-ToF-MS monoterpene sensitivity is weighed by a speciation profile from TOGA measurements (Section 2.2.2; Equation 2). However, the factor of 5 difference here is much larger than can reasonably be explained by differences in calibration factor alone as it would require unrealistic sensitivities. Finally, in addition to other monoterpene isomers, the high PTR-ToF-MS monoterpene measurement may have a contribution from interfering fragments of higher-mass species such as bornyl acetate (Hatch et al., 2017).

PTR-ToF-MS measured furan ~1.5 times higher than TOGA with an r^2 of 0.814, potentially suggesting an unknown additional isomer detected by PTR-ToF-MS or a loss in the GC system. Methylfurans were measured by PTR-ToF-MS to be ~15 times greater than the sum of isomers measured by TOGA. Though the PTR-ToF-MS measurement was corrected for being 37% fragmentary at this mass following Koss et al. (2018), the cause of this discrepancy is currently unknown. Finally, the sum of C_9 aromatics measured by AWAS was found to be ~4 times greater than PTR-ToF-MS (not shown in Figure 2 to preserve *y*-axis scale). As the PTR-ToF-MS was calibrated using 1,3,5- and 1,2,4-trimethylbenzene, this may indicate a significant proportion of other substituted C_9 aromatics undergo fragmentation in the drift tube, potentially biasing the PTR-ToF-MS C_9 aromatic measurement low.

For PTR-ToF-MS ion masses with only calculated calibration factors, acrylonitrile, propanenitrile, and acrolein measured by TOGA were found to agree within the combined measurement uncertainty of <60%. AWAS measured propene was observed to be 2.5 times higher than measured by PTR-ToF-MS, potentially due to overcorrecting the amount of that mass attributed to fragments (not shown in Figure 2 to preserve the *y*-axis scale). TOGA-measured styrene was found to be ~4 times lower than PTR-ToF-MS, and the reason for this discrepancy is currently unknown. AWAS propene and TOGA styrene are reported in this work rather than PTR-ToF-MS (Section 2.4).

Due to different sampling frequencies, TOGA and AWAS mixing ratios cannot be directly compared as in Figure 2. Instead, we compare ERs for 15 "unique fires" where both TOGA and AWAS capture the same plume transect (Figure S3). All TOGA and AWAS co-measured ERs except 3-methylpentane agree within <50%, with most <30%. The poor slope comparison for 3-methylpentane is due in part to it being only slightly enhanced in the wildfires compared to the other observed alkanes. Though slopes for the reduced major axis regression between TOGA and AWAS ERs agree well, correlation coefficients and standard errors are generally worse than in Figure 2 due to added uncertainty from the CO measurement, background corrections, and sampling of different locations within a plume.

During WE-CAN, 48% of the measured mass (sum of VOC EFs) was directly calibrated in the PTR-ToF-MS, emphasizing that the strength of the technique is largely dependent on the ability to get accurate sensitivities for non-directly calibrated VOCs. PTR-ToF-MS is further challenged by a lack of speciation information for wildfire smoke, which likely contributes to discrepancies when comparing to TOGA or AWAS measurements (Figure 2). However, the high temporal resolution (<1 s) of PTR-ToF-MS allows for narrow smoke plumes with rapid changes in VOC concentrations to be captured (Müller et al., 2016), while TOGA is constrained by the time needed for gas chromatography separation (~100 s). Though AWAS theoretically has little temporal limitations between filling consecutive canisters, the discrete number of canisters available per flight makes it difficult to capture every plume transect while still sufficiently characterizing background air. As most plumes were crossed in 1–4 min at the emission transect and most flights had tens or more transects through smoke, of the 31 emission transects identified in this work only 20 were sampled by TOGA and 20 by AWAS. Together, the large number of VOCs measured by PTR-ToF-MS, coupled with the speciation power, low detection limits, and characterization of alkanes, alkenes, nitrogen-containing VOCs, and halides of AWAS and TOGA greatly improves our ability to characterize wildfire emission during WE-CAN. If each instrument were deployed to sample fire emissions alone, a PTR-ToF-MS would capture 87% of the measured VOC mass during WE-CAN (Section 7.2), while AWAS and TOGA capture 34% and 38% respectively. These proportions are somewhat consistent with the proportions reported from laboratory burns (Hatch et al., 2017). Of the fraction captured by AWAS, 65% are alkenes, aldehydes, and alkanes. Similarly, 65% of the TOGA fraction consists of aldehydes, alcohols, and aromatics.

5. Emission Factors for Speciated and Total VOCs

Table 2 shows WE-CAN campaign-averaged ERs and EFs for 161 VOCs/ion masses, OC, BC, CH_4, CO, and CO_2. Additional speciation is also provided for 30 isomers known to contribute to PTR-ToF-MS ion masses (Section 2.4). Fire-to-fire variability is reflected by the standard deviation of the study average (1σ). One challenge of airborne emission sampling is that the nearest plume transect to a given fire is often tens of minutes or more from the source due to plane safety and firefighting traffic concerns (average aging 60 ± 40 min in WE-CAN; Table 1). For reactive species that are not photochemically produced in the outflow from fires such as monoterpenes or furan, the EF is likely a lower limit. For reactive species that are both directly emitted and photochemically produced in the outflow such as formaldehyde or acetaldehyde, the EF reported here represents the sum of the fraction remaining after decay experienced before the time of analysis and the fraction formed in the plume from precursors. To maximize sample numbers and improve statistics, here we choose to include all emission transects available and focus on discussing the campaign average with the potential aging effect reflected in part by the deviation. Additionally, EFs that include slight aging may be more appropriate for the spatial and temporal resolution in many models (Lonsdale et al., 2020). A more detailed breakdown of EFs and ERs by fire/transect with corresponding estimated physical age and MCE can be found in the supplement (Tables S2 and S3).

For the western U.S. wildfires sampled during WE-CAN, the total measured mass of VOCs emitted per fire (expressed as the total EF of all measured VOCs, or $tVOC_{EF}$) ranges from 9.8 to 35.9 g kg^{-1}, with a mean EF of 26.1 ± 6.9 g kg^{-1} (1σ). Our average $tVOC_{EF}$ is consistent with many previous studies including (1) an early estimate of total non-methane organic gases (NMOG) for temperate forest fires (23.7 g kg^{-1}; Akagi et al., 2011), (2) total NMOG for pine-forest understory prescribed fires (27.6 g kg^{-1}; Yokelson et al., 2013), (3) total NMOG from FLAME-4 laboratory coniferous canopy fires (23.9 g kg^{-1}; Stockwell et al., 2015) and (4) the total PTR-ToF-MS measured NMOG for carefully simulated wildfires in FIREX-MFL (25.0 g kg^{-1}; Koss et al., 2018).

On a molar basis, the total measured VOC emitted by western U.S. wildfires relative to CO (sum of ERs) ranges from 90.0 to 206.1 ppbv $ppmv^{-1}$, with an average of 148.3 ± 29.6 ppbv $ppmv^{-1}$. This sum of ERs is also similar to the laboratory-determined sum of 144.5 ppbv $ppmv^{-1}$ for western U.S. fuels (Koss et al., 2018). We later conduct a detailed comparison with previous field and laboratory studies exploring the ability of flaming versus smoldering combustion processes to explain variability in total measured VOC emissions (Section 7).

On average, the top 10 most abundantly emitted species (discussed collectively as individual isomers measured by GC and speciated ion masses representing 1–3 isomers measured by PTR-ToF-MS) account for ~53%

Table 2
WE-CAN Campaign-Averaged Emission Ratios, Emission Factors, and VOC Mass Fractions

VOC contributor[a]	Exact Mass[b], Da	Chemical Formula	N[c]	ER to CO, ppb ppm^{-1} (σ)	EF, g kg^{-1} (σ)	VOC Mass Fraction, %
Carbon dioxide	43.990	CO_2	24	9,520.00 (2,500.00)	1,413.00 (61.00)	–
Carbon monoxide	27.995	CO	24	1,000.00 (–)	99.30 (20.00)	–
Methane	16.031	CH_4	24	102.00 (17.00)	5.93 (1.80)	–
Ethyne[d]	26.016	C_2H_2	16	3.50 (1.80)	0.31 (0.17)	1.20 (0.71)
Hydrogen cyanide[e]	27.011	HCN	15	4.30 (1.70)	0.43 (0.17)	1.70 (0.79)
Ethene[d]	28.031	C_2H_4	16	16.00 (9.10)	1.50 (1.00)	5.90 (4.20)
Formaldehyde	30.011	CH_2O	24	18.00 (3.30)	1.90 (0.43)	7.30 (2.50)
Ethane[d]	30.047	C_2H_6	16	10.00 (6.70)	1.10 (0.84)	4.30 (3.40)
Methanol	32.026	CH_4O	24	13.00 (2.00)	1.50 (0.39)	5.80 (2.10)
Acetonitrile	41.027	C_2H_3N	24	2.10 (0.99)	0.31 (0.15)	1.20 (0.65)
Propene[d]	42.047	C_3H_6	16	4.90 (3.60)	0.74 (0.62)	2.90 (2.50)
Isocyanic acid	43.006	HNCO	24	1.10 (0.35)	0.16 (0.036)	0.61 (0.21)
Ethenamine	43.042	C_2H_5N	24	0.072 (0.034)	0.011 (0.0058)	0.043 (0.025)
Acetaldehyde	44.026	C_2H_4O	24	11.00 (1.60)	1.70 (0.43)	6.30 (2.30)
Propane[e]	44.063	C_3H_8	15	2.70 (0.92)	0.46 (0.18)	1.80 (0.84)
Formamide	45.021	CH_3NO	24	0.23 (0.08)	0.037 (0.014)	0.14 (0.066)
Formic acid[f]	46.005	CH_2O_2	20	9.50 (4.20)	1.50 (0.60)	5.70 (2.70)
Ethanol[e]	46.042	C_2H_6O	13	0.19 (0.17)	0.035 (0.04)	0.13 (0.16)
Methyl chloride[e]	49.992	CH_3Cl	15	0.092 (0.047)	0.017 (0.0089)	0.067 (0.038)
1-Buten-3-yne	52.031	C_4H_4	24	0.28 (0.088)	0.052 (0.018)	0.20 (0.087)
Acrylonitrile	53.027	C_3H_3N	24	0.23 (0.076)	0.044 (0.015)	0.17 (0.074)
2-Propynal	54.011	C_3H_2O	24	0.20 (0.089)	0.037 (0.015)	0.14 (0.07)
1,3-Butadiene, 1,2-Butadiene	54.047	C_4H_6	24	1.40 (0.38)	0.27 (0.096)	1.00 (0.46)
Propanenitrile	55.042	C_3H_5N	24	0.19 (0.087)	0.037 (0.018)	0.14 (0.077)
Acrolein[e]	56.026	C_3H_4O	15	1.90 (0.66)	0.40 (0.18)	1.50 (0.79)
Butenes	56.063	C_4H_8	24	1.30 (0.52)	0.26 (0.12)	1.00 (0.52)
Isobutene, 1-Butene[e]	56.063	C_4H_8	15	1.30 (0.78)	0.28 (0.17)	–
Methyl isocyanate, Hydroxyacetonitrile	57.021	C_2H_3NO	24	0.16 (0.03)	0.033 (0.0087)	0.13 (0.047)
Propeneamines	57.058	C_3H_7N	24	0.087 (0.035)	0.018 (0.0082)	0.07 (0.037)
Glyoxal	58.005	$C_2H_2O_2$	22	0.028 (0.023)	0.0054 (0.0045)	0.021 (0.018)
Acetone, Propanal	58.042	C_3H_6O	24	4.10 (0.64)	0.84 (0.22)	3.20 (1.20)
Acetone[e]	58.042	C_3H_6O	15	2.90 (1.40)	0.65 (0.38)	–
Propanal[e]	58.042	C_3H_6O	15	0.81 (0.30)	0.18 (0.07)	–
n-Butane[e]	58.078	C_4H_{10}	15	0.56 (0.26)	0.12 (0.061)	0.48 (0.27)
Isobutane[e]	58.078	C_4H_{10}	15	0.17 (0.088)	0.038 (0.019)	0.14 (0.084)
Acetamide	59.037	C_2H_5NO	24	0.19 (0.046)	0.04 (0.012)	0.15 (0.061)
Trimethylamine	59.073	C_3H_9N	24	0.026 (0.0085)	0.0054 (0.002)	0.021 (0.0095)
Acetic acid, Glycolaldehyde (=hydroxyacetaldehyde)	60.021	$C_2H_4O_2$	24	11.00 (2.10)	2.40 (0.61)	9.40 (3.40)
Isopropanol[e]	60.058	C_3H_8O	14	0.032 (0.021)	0.0074 (0.0058)	0.028 (0.024)
Nitromethane	61.016	CH_3NO_2	24	0.38 (0.10)	0.078 (0.0085)	0.30 (0.085)
Dimethyl sulfide[d]	62.019	C_2H_6S	9	0.41 (0.37)	0.08 (0.083)	0.31 (0.33)

Table 2
Continued

VOC contributor[a]	Exact Mass[b], Da	Chemical Formula	N[c]	ER to CO, ppb ppm^{-1} (σ)	EF, g kg^{-1} (σ)	VOC Mass Fraction, %
Cyanoallene isomers	65.027	C_4H_3N	24	0.0074 (0.0055)	0.0017 (0.0012)	0.0064 (0.0049)
1,3-Cyclopentadiene	66.047	C_5H_6	24	0.048 (0.018)	0.011 (0.0049)	0.044 (0.022)
Pyrrole, Butenenitrile isomers	67.042	C_4H_5N	24	0.16 (0.091)	0.039 (0.021)	0.15 (0.089)
Methacrylonitrile[e]	67.042	C_4H_5N	15	0.056 (0.043)	0.014 (0.011)	–
Carbon suboxide	67.990	C_3O_2	21	0.037 (0.024)	0.0084 (0.0054)	0.032 (0.023)
Furan	68.026	C_4H_4O	24	1.70 (0.60)	0.43 (0.19)	1.70 (0.85)
Isoprene[e]	68.063	C_5H_8	15	0.31 (0.39)	0.082 (0.095)	0.31 (0.37)
Butanenitriles, Dihydropyrrole	69.058	C_4H_7N	24	0.081 (0.04)	0.02 (0.01)	0.077 (0.044)
Propiolic acid	70.005	$C_3H_2O_2$	23	0.044 (0.029)	0.011 (0.0071)	0.041 (0.029)
Methyl vinyl ketone, Methacrolein, 2-Butenal (=crotonaldehyde)	70.042	C_4H_6O	24	1.60 (0.51)	0.39 (0.15)	1.50 (0.71)
Methyl vinyl ketone[e]	70.042	C_4H_6O	15	0.75 (0.45)	0.20 (0.12)	–
Methacrolein[e]	70.042	C_4H_6O	15	0.37 (0.26)	0.097 (0.067)	–
2-Butenal[e]	70.042	C_4H_6O	15	0.15 (0.075)	0.041 (0.02)	–
Pentenes, Methylbutenes	70.078	C_5H_{10}	24	0.06 (0.03)	0.015 (0.0084)	0.059 (0.036)
Cyclopentane[d]	70.078	C_5H_{10}	16	0.014 (0.0088)	0.0035 (0.0025)	–
Buteneamines, Tetrahydropyrrole	71.073	C_4H_9N	21	0.014 (0.011)	0.0036 (0.003)	0.014 (0.012)
Pyruvaldehyde (=methyl glyoxal), Acrylic acid	72.021	$C_3H_4O_2$	24	0.84 (0.26)	0.22 (0.082)	0.83 (0.39)
Methyl ethyl ketone, 2-Methylpropanal, Butanal	72.058	C_4H_8O	24	0.82 (0.17)	0.21 (0.063)	0.81 (0.32)
Methyl ethyl ketone[e]	72.058	C_4H_8O	15	0.73 (0.27)	0.20 (0.075)	–
Butanal[e]	72.058	C_4H_8O	15	0.19 (0.079)	0.053 (0.023)	–
n-Pentane[e]	72.094	C_5H_{12}	15	0.21 (0.094)	0.057 (0.028)	0.22 (0.12)
Isopentane[e]	72.094	C_5H_{12}	15	0.069 (0.043)	0.019 (0.012)	0.073 (0.05)
Nitroethene	73.016	$C_2H_3NO_2$	24	0.038 (0.013)	0.0099 (0.0037)	0.038 (0.017)
Hydroxyacetone, Methyl acetate, Ethyl formate	74.037	$C_3H_6O_2$	24	2.10 (0.57)	0.57 (0.20)	2.20 (0.97)
Nitroethane, Ethyl nitrite	75.032	$C_2H_5NO_2$	24	0.045 (0.012)	0.012 (0.0042)	0.047 (0.02)
Carbon disulfide[e]	75.944	CS_2	15	0.0016 (0.0012)	4.5e-04 (3.1e-04)	0.0017 (0.0013)
Benzene	78.047	C_6H_6	24	1.80 (0.24)	0.50 (0.14)	1.90 (0.73)
Pentadienenitriles, Pyridine	79.042	C_5H_5N	24	0.13 (0.025)	0.037 (0.01)	0.14 (0.055)
2,4-Cyclopentadiene-1-one	80.026	C_5H_4O	24	0.092 (0.052)	0.027 (0.017)	0.11 (0.07)
Pentenenitriles, Methylpyrroles	81.058	C_5H_7N	24	0.069 (0.039)	0.02 (0.011)	0.077 (0.048)
2-Methylfuran, 3-Methylfuran	82.042	C_5H_6O	24	0.92 (0.38)	0.28 (0.13)	1.10 (0.58)
2-Methylfuran[e]	82.042	C_5H_6O	12	0.15 (0.09)	0.047 (0.03)	–
3-Methylfuran[e]	82.042	C_5H_6O	14	0.03 (0.021)	0.0097 (0.0071)	–
2,2-Dimethylbutane[d]	82.078	C_6H_{10}	14	0.055 (0.037)	0.015 (0.011)	0.058 (0.043)
Pentanenitriles	83.073	C_5H_9N	24	0.071 (0.037)	0.021 (0.011)	0.08 (0.047)
Dichloromethane[e]	83.953	CH_2Cl_2	14	0.0088 (0.0064)	0.0029 (0.0022)	0.011 (0.009)
2(3H)-Furanone	84.021	$C_4H_4O_2$	24	1.10 (0.28)	0.32 (0.11)	1.20 (0.54)
3-Methyl-3-buten-2-one, Cyclopentanone	84.058	C_5H_8O	24	0.28 (0.099)	0.087 (0.038)	0.33 (0.17)
Cyclohexane[d]	84.094	C_6H_{12}	6	0.026 (0.043)	0.008 (0.014)	0.031 (0.055)
2,3-Butanedione, Methyl acrylate	86.037	$C_4H_6O_2$	24	1.70 (0.52)	0.53 (0.21)	2.00 (0.97)

Table 2
Continued

VOC contributor[a]	Exact Mass[b], Da	Chemical Formula	N[c]	ER to CO, ppb ppm^{-1} (σ)	EF, g kg^{-1} (σ)	VOC Mass Fraction, %
3-Methyl-2-butanone, 2-Pentanone, 3-Pentanone, 2-Methylbutanal, 3-Methylbutanal	86.073	$C_5H_{10}O$	24	0.20 (0.058)	0.062 (0.023)	0.24 (0.11)
2-Methyl-3-buten-2-ol[e]	86.073	$C_5H_{10}O$	13	0.018 (0.01)	0.0061 (0.0036)	–
n-Hexane[d]	86.110	C_6H_{14}	15	0.13 (0.10)	0.04 (0.036)	0.15 (0.14)
3-Methylpentane[d]	86.110	C_6H_{14}	12	0.034 (0.019)	0.01 (0.0065)	0.039 (0.027)
Pyruvic acid	88.016	$C_3H_4O_3$	22	0.063 (0.026)	0.019 (0.008)	0.074 (0.036)
Methyl propanoate	88.052	$C_4H_8O_2$	24	0.25 (0.094)	0.081 (0.036)	0.31 (0.16)
Nitropropanes	89.048	$C_3H_7NO_2$	23	0.0074 (0.0033)	0.0024 (0.0012)	0.0092 (0.0052)
2,4-Dimethylpentane[d]	90.047	C_7H_{16}	7	0.0076 (0.0094)	0.0023 (0.003)	0.0086 (0.012)
Ethylnylpyrrole	91.042	C_6H_5N	24	0.028 (0.0068)	0.0091 (0.0026)	0.035 (0.014)
Toluene	92.063	C_7H_8	24	1.20 (0.33)	0.42 (0.16)	1.60 (0.74)
3-Furancarbonitrile, 2-Furancarbonitrile	93.021	C_5H_3NO	24	0.026 (0.0087)	0.0088 (0.0037)	0.034 (0.017)
2-Methylpyridine, 3-Methylpyridine	93.058	C_6H_7N	24	0.10 (0.026)	0.035 (0.012)	0.13 (0.057)
Methyl bromide[e]	93.942	CH_3Br	14	0.0029 (0.002)	1e-03 (7.1e-04)	0.0039 (0.0029)
Phenol	94.042	C_6H_6O	24	0.98 (0.34)	0.33 (0.13)	1.30 (0.60)
2-Furfural (=furaldehyde), 3-Furfural	96.021	$C_5H_4O_2$	24	1.50 (0.44)	0.53 (0.21)	2.00 (0.97)
C$_2$-Substituted furan isomers, 2,5-Dimethylfuran, 2-Ethylfuran	96.058	C_6H_8O	24	0.57 (0.25)	0.20 (0.096)	0.77 (0.42)
4-Methylpentanenitrile	97.089	$C_6H_{11}N$	24	0.025 (0.014)	0.0088 (0.0047)	0.034 (0.02)
1,2-Dichloroethane[e]	97.969	$C_2H_4Cl_2$	10	0.002 (0.0022)	8.2e-04 (9.1e-04)	0.0032 (0.0036)
Maleic anhydride	98.000	$C_4H_2O_3$	24	0.44 (0.28)	0.14 (0.072)	0.55 (0.31)
2-Furanmethanol	98.037	$C_5H_6O_2$	24	0.25 (0.10)	0.09 (0.043)	0.34 (0.19)
$C_6H_{10}O$ Ketones, Methylcyclopentanone, Cyclohexanone	98.073	$C_6H_{10}O$	24	0.096 (0.033)	0.034 (0.015)	0.13 (0.066)
Methylcyclohexane[d]	98.110	C_7H_{14}	13	0.05 (0.059)	0.018 (0.022)	0.07 (0.088)
Dihydrofurandione	100.016	$C_4H_4O_3$	23	0.16 (0.059)	0.055 (0.019)	0.21 (0.092)
Methyl methacrylate	100.052	$C_5H_8O_2$	24	0.31 (0.098)	0.11 (0.045)	0.44 (0.21)
Hexanones, Hexanal	100.089	$C_6H_{12}O$	23	0.036 (0.011)	0.013 (0.0056)	0.05 (0.025)
n-Heptane[d]	100.125	C_7H_{16}	16	0.13 (0.13)	0.046 (0.05)	0.18 (0.20)
2-Methylhexane[d]	100.125	C_7H_{16}	9	0.057 (0.11)	0.021 (0.042)	0.079 (0.16)
3-Methylhexane[d]	100.125	C_7H_{16}	5	0.04 (0.046)	0.016 (0.018)	0.06 (0.072)
2,3-Dimethylpentane[d]	100.125	C_7H_{16}	10	0.011 (0.019)	0.0039 (0.0075)	0.015 (0.029)
Acetic anhydride	102.032	$C_4H_6O_3$	24	0.12 (0.04)	0.044 (0.02)	0.17 (0.088)
Benzonitrile	103.042	C_7H_5N	24	0.15 (0.053)	0.055 (0.022)	0.21 (0.10)
Styrene[e]	104.063	C_8H_8	15	0.045 (0.028)	0.018 (0.012)	0.07 (0.048)
Isopropyl nitrate[e]	105.043	$C_3H_7NO_3$	13	0.0033 (0.0014)	0.0013 (5.5e−04)	0.0049 (0.0025)
n-Propyl nitrate	105.043	$C_3H_7NO_3$	4	0.0015 (6.5e-04)	5.3e-04 (2.4e-04)	0.002 (0.0011)
Vinylpyridine	105.058	C_7H_7N	24	0.022 (0.0092)	0.0085 (0.0038)	0.033 (0.017)
Benzaldehyde	106.042	C_7H_6O	24	0.22 (0.043)	0.084 (0.026)	0.32 (0.13)
C$_8$ Aromatics	106.078	C_8H_{10}	24	0.53 (0.17)	0.21 (0.08)	0.79 (0.37)
(m,p)-Xylenes[e]	106.078	C_8H_{10}	15	0.16 (0.077)	0.065 (0.033)	–
Ethylbenzene[e]	106.078	C_8H_{10}	15	0.12 (0.046)	0.05 (0.022)	–
o-Xylene[e]	106.078	C_8H_{10}	15	0.062 (0.028)	0.025 (0.012)	–

Table 2
Continued

VOC contributor[a]	Exact Mass[b], Da	Chemical Formula	N[c]	ER to CO, ppb ppm^{-1} (σ)	EF, g kg^{-1} (σ)	VOC Mass Fraction, %
Quinone (=p-benzoquinone)	108.021	$C_6H_4O_2$	24	0.20 (0.049)	0.077 (0.02)	0.30 (0.11)
2-Methylphenol (=o-Cresol), Anisol	108.058	C_7H_8O	24	0.57 (0.25)	0.23 (0.11)	0.87 (0.49)
5-Methylfurfural, Benzene diols (=catechol, resorcinol)	110.037	$C_6H_6O_2$	24	0.62 (0.24)	0.25 (0.12)	0.96 (0.52)
C_3 Furans	110.073	$C_7H_{10}O$	24	0.11 (0.052)	0.046 (0.024)	0.18 (0.10)
Dihydroxy pyridine, Methyl maleimide	111.032	$C_5H_5NO_2$	24	0.06 (0.017)	0.024 (0.0084)	0.092 (0.04)
Chlorobenzene[e]	112.008	C_6H_5Cl	14	4.5e-04 (2.4e-04)	2e-04 (1.3e-04)	7.5e-04 (5.2e-04)
5-Hydroxy-2-furfural/2-furoic acid	112.016	$C_5H_4O_3$	24	0.32 (0.07)	0.12 (0.031)	0.48 (0.17)
2-Hydroxy-3-methyl-2-cyclopenten-1-one	112.052	$C_6H_8O_2$	24	0.29 (0.13)	0.12 (0.061)	0.46 (0.26)
Ethylcyclopentanone	112.089	$C_7H_{12}O$	24	0.034 (0.016)	0.014 (0.007)	0.053 (0.03)
Nitrofuran	113.011	$C_4H_3NO_3$	24	0.013 (0.0044)	0.0051 (0.0019)	0.019 (0.0088)
5-Hydroxymethyl-2[3H]-furanone	114.032	$C_5H_6O_3$	24	0.063 (0.024)	0.026 (0.011)	0.098 (0.049)
C_6 1-DBE esters, C_6 Diones	114.068	$C_6H_{10}O_2$	24	0.093 (0.032)	0.039 (0.017)	0.15 (0.076)
Heptanal, 2,4-Dimethyl-3-pentanone, Heptanone	114.104	$C_7H_{14}O$	24	0.017 (0.0048)	0.0072 (0.0025)	0.027 (0.012)
2,2,4-Trimethylpentane[d]	114.141	C_8H_{18}	13	0.071 (0.046)	0.028 (0.018)	0.11 (0.073)
n-Octane[d]	114.141	C_8H_{18}	15	0.052 (0.038)	0.021 (0.017)	0.082 (0.07)
2-Methylheptane[d]	114.141	C_8H_{18}	14	0.034 (0.11)	0.015 (0.048)	0.056 (0.18)
2,3,4-Trimethylpentane[d]	114.141	C_8H_{18}	3	0.015 (0.021)	0.0067 (0.01)	0.026 (0.04)
3-Methylheptane[d]	114.141	C_8H_{18}	6	0.017 (0.022)	0.0074 (0.01)	0.028 (0.04)
5-Hydroxymethyl tetrahydro 2-furanone, 5-Hydroxy tetrahydro 2-furfural	116.047	$C_5H_8O_3$	24	0.08 (0.038)	0.034 (0.019)	0.13 (0.08)
C_6 Esters	116.084	$C_6H_{12}O_2$	24	0.028 (0.015)	0.011 (0.0062)	0.044 (0.026)
Benzeneacetonitrile	117.058	C_8H_7N	24	0.023 (0.0071)	0.0096 (0.0034)	0.037 (0.016)
Chloroform[e]	117.914	$CHCl_3$	7	7.5e-04 (5.9e-04)	3.6e-04 (2.9e-04)	0.0014 (0.0012)
Benzofuran	118.042	C_8H_6O	24	0.096 (0.028)	0.041 (0.015)	0.16 (0.072)
Methylstyrenes, Indane, Propenylbenzenes	118.078	C_9H_{10}	24	0.086 (0.041)	0.037 (0.019)	0.14 (0.081)
Isobutyl nitrate, 2-Butyl nitrate[e]	119.058	$C_4H_9NO_3$	7	0.0047 (0.0029)	0.0019 (0.0011)	0.0073 (0.0048)
Tolualdehydes	120.058	C_8H_8O	24	0.19 (0.053)	0.082 (0.03)	0.31 (0.14)
C_9 Aromatics	120.094	C_9H_{12}	24	0.16 (0.064)	0.069 (0.031)	0.26 (0.14)
1,2,3-Trimethylbenzene[d]	120.094	C_9H_{12}	16	0.19 (0.23)	0.089 (0.11)	–
1,2,4-Trimethylbenzene[d]	120.094	C_9H_{12}	15	0.17 (0.21)	0.076 (0.099)	–
4-Ethyltoluene[d]	120.094	C_9H_{12}	14	0.10 (0.15)	0.045 (0.071)	–
3-Ethyltoluene[d]	120.094	C_9H_{12}	14	0.079 (0.098)	0.034 (0.046)	–
2-Ethyltoluene[d]	120.094	C_9H_{12}	14	0.058 (0.11)	0.025 (0.051)	–
Isopropylbenzene[d]	120.094	C_9H_{12}	13	0.03 (0.054)	0.013 (0.025)	–
n-Propylbenzene[d]	120.094	C_9H_{12}	12	0.015 (0.0084)	0.0064 (0.0039)	–
1,3,5-Trimethylbenzene[d]	120.094	C_9H_{12}	7	0.0085 (0.0069)	0.0036 (0.0027)	–
2-Hydroxybenzaldehyde (=salicylaldehyde)	122.037	$C_7H_6O_2$	24	0.15 (0.041)	0.065 (0.023)	0.25 (0.11)
C_2 Phenols, Methyl anisol	122.073	$C_8H_{10}O$	24	0.22 (0.11)	0.10 (0.057)	0.39 (0.24)
Hydroxybenzoquinone	124.016	$C_6H_4O_3$	24	0.098 (0.052)	0.045 (0.026)	0.17 (0.11)
Guaiacol (=2-methoxyphenol)	124.052	$C_7H_8O_2$	24	0.58 (0.32)	0.27 (0.17)	1.00 (0.70)
5-(Hydroxymethyl)-2-furfural	126.032	$C_6H_6O_3$	24	0.14 (0.047)	0.064 (0.026)	0.24 (0.12)

Table 2
Continued

VOC contributor[a]	Exact Mass[b], Da	Chemical Formula	N[c]	ER to CO, ppb ppm^{-1} (σ)	EF, g kg^{-1} (σ)	VOC Mass Fraction, %
n-Nonane[d]	128.156	C_9H_{20}	15	0.033 (0.024)	0.015 (0.012)	0.058 (0.048)
1,1,1-Trichloroethane[e]	131.930	$C_2H_3Cl_3$	12	4.3e−04 (6.5e−04)	2.1e−04 (3.2e−04)	8.2e−04 (0.0012)
Methylbenzofurans	132.058	C_9H_8O	24	0.094 (0.036)	0.046 (0.021)	0.17 (0.092)
Ethyl styrenes, Methylpropenylbenzenes, Butenylbenzenes	132.094	$C_{10}H_{12}$	24	0.083 (0.053)	0.04 (0.026)	0.15 (0.11)
3-Methylacetophenone	134.073	$C_9H_{10}O$	24	0.092 (0.034)	0.045 (0.019)	0.17 (0.086)
C_{10} Aromatics	134.110	$C_{10}H_{14}$	24	0.081 (0.039)	0.04 (0.021)	0.15 (0.09)
Methylbenzoic acid	136.052	$C_8H_8O_2$	24	0.13 (0.047)	0.066 (0.029)	0.25 (0.13)
Monoterpenes	136.125	$C_{10}H_{16}$	24	0.41 (0.30)	0.21 (0.15)	0.79 (0.61)
Camphene[e]	136.125	$C_{10}H_{16}$	15	0.03 (0.021)	0.016 (0.011)	–
α-Pinene[e]	136.125	$C_{10}H_{16}$	15	0.026 (0.02)	0.014 (0.012)	–
β-Pinene, Myrcene[e]	136.125	$C_{10}H_{16}$	10	0.021 (0.014)	0.011 (0.0079)	–
Tricyclene[e]	136.125	$C_{10}H_{16}$	15	0.0047 (0.0032)	0.0025 (0.0018)	–
Nitrotoluene	137.048	$C_7H_7NO_2$	23	0.014 (0.0057)	0.0071 (0.0034)	0.027 (0.015)
2-Methoxy-4-methylphenol (=creosol)	138.068	$C_8H_{10}O_2$	24	0.27 (0.18)	0.14 (0.11)	0.54 (0.44)
Methyl iodide[e]	141.928	CH_3I	15	0.0014 (7e−04)	7.7e−04 (5.2e−04)	0.0029 (0.0022)
Methylnaphthalene	142.078	$C_{11}H_{10}$	24	0.096 (0.041)	0.05 (0.024)	0.19 (0.10)
Product of levoglucosan dehydration (pyrolysis)	144.042	$C_6H_8O_4$	24	0.078 (0.052)	0.042 (0.03)	0.16 (0.12)
Dimethylbenzofuran	146.073	$C_{10}H_{10}O$	24	0.095 (0.047)	0.051 (0.028)	0.20 (0.12)
Methyl chavicol (=estragole)	148.089	$C_{10}H_{12}O$	24	0.046 (0.026)	0.025 (0.015)	0.097 (0.062)
C_{11} Aromatics	148.125	$C_{11}H_{16}$	24	0.025 (0.013)	0.014 (0.0074)	0.052 (0.031)
Vinyl guaiacol	150.068	$C_9H_{10}O_2$	24	0.063 (0.041)	0.036 (0.025)	0.14 (0.10)
Vanillin	152.047	$C_8H_8O_3$	18	0.04 (0.041)	0.022 (0.023)	0.083 (0.092)
Oxygenated monoterpenes, Camphor	152.120	$C_{10}H_{16}O$	24	0.045 (0.027)	0.025 (0.014)	0.094 (0.059)
Syringol	154.063	$C_8H_{10}O_3$	24	0.03 (0.011)	0.017 (0.0067)	0.065 (0.031)
Cineole, Other oxygenated monoterpenes	154.136	$C_{10}H_{18}O$	24	0.0048 (0.0029)	0.0027 (0.0017)	0.01 (0.0071)
1,3-Dimethylnaphthalene	156.094	$C_{12}H_{12}$	24	0.051 (0.027)	0.03 (0.018)	0.12 (0.074)
Decanal	156.151	$C_{10}H_{20}O$	21	0.0067 (0.0031)	0.0037 (0.0017)	0.014 (0.0076)
C_{12} Aromatics	162.141	$C_{12}H_{18}$	24	0.01 (0.0061)	0.0062 (0.0036)	0.024 (0.015)
Eugenol, Isoeugenol	164.084	$C_{10}H_{12}O_2$	24	0.032 (0.021)	0.02 (0.014)	0.076 (0.058)
C_{13} Aromatics	176.156	$C_{13}H_{20}$	24	0.013 (0.0065)	0.0085 (0.0047)	0.033 (0.02)
Sesquiterpenes	204.188	$C_{15}H_{24}$	23	0.038 (0.038)	0.029 (0.028)	0.11 (0.11)
Black carbon[g]	–	–	24	4.95 (2.00)[i]	0.389 (0.17)	–
Organic carbon[h]	–	–	24	145.00 (23.00)[i]	11.60 (3.30)	–
Total VOC emissions				**148.26 (29.61)**	**26.11 (6.92)**	

Further details such as breakdown by fire and regression coefficients between MCE and EF are available in the Supporting Information.

Note. Uncertainties are reported as the standard deviation (1σ) of the campaign average, representing fire-to-fire variability. The corresponding campaign average MCE is 0.90.

[a]VOC contributors to PTR-ToF-MS measured ion masses are assigned based on Koss et al. (2018) and listed in order of most abundant isomeric contribution. Italicized VOC contributors are shown for speciation purposes but not included in the total carbon term of the carbon mass balance nor total emissions calculations (Section 2.4). [b]Dominant/Primary isotopologue exact mass; protonated mass is the exact mass plus 1.0203. [c]Number of emission transects sampled more than 30 min apart. [d]Advanced whole air sampler (AWAS). [e]Trace organic gas analyzer (TOGA). [f]Iodide-adduct time-of-flight chemical-ionization mass (I$^-$ CIMS). [g]Single particle soot photometer (SP2). [h]High-resolution aerosol mass spectrometer (HR-AMS). [i]µg sm^{-3} ppm^{-1} CO.
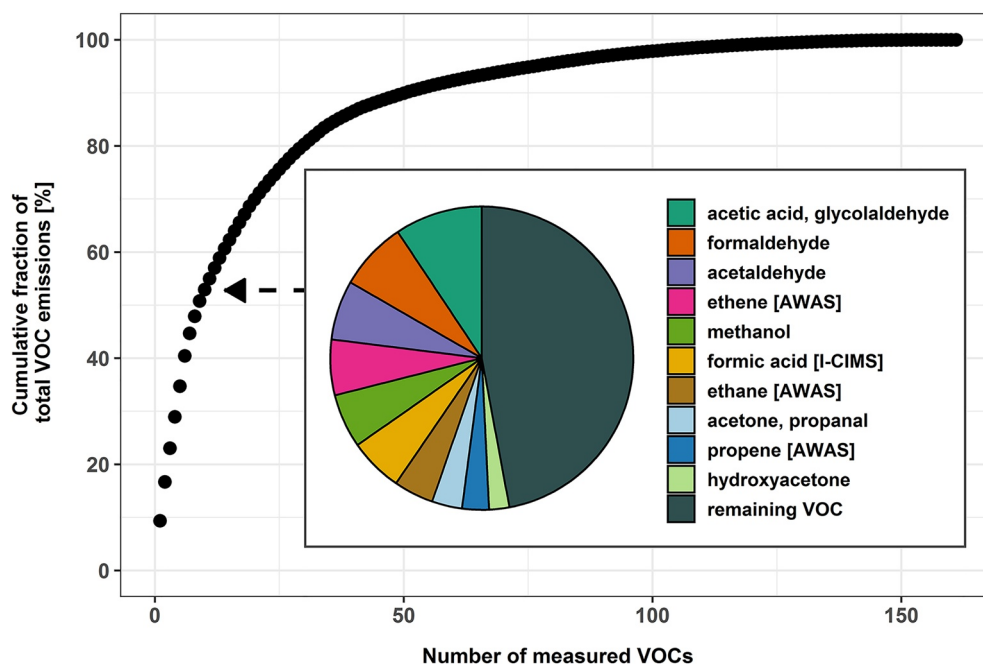
Figure 3. The cumulative mass fraction of the total measured VOC emissions as a function of measured VOCs during WE-CAN. 76 VOCs account for 95% of the total measured VOC mass, and 117 VOCs account for 99% of the total measured VOC mass. The inset pie chart shows the 10 most abundantly emitted VOCs which account for ~53% of the total mass emitted, while the remaining mass consists of 151 species. Reported species not measured by PTR-ToF-MS are identified by corresponding instrument in the legend (i.e., Ethene [AWAS]). Note that hydroxyacetone also includes methyl acetate and ethyl formate isomers (Koss et al., 2018).

of the tVOC$_{EF}$ in western U.S. wildfire smoke, or ~68% on a molar basis (Figure 3). The remaining 47% of VOC mass is represented by at least 151 species each individually contributing less than 2% to the overall tVOC$_{EF}$. In contrast, 15 species were needed to reach 50% of the total measured VOC EF in FIREX-MFL (Koss et al., 2018), likely due to the inclusion of ethane in this work, as well as the higher acetaldehyde, ethene, formic acid, and acetone EFs observed during WE-CAN relative to FIREX-MFL. Many of the most abundantly emitted VOCs have also been reported as top emissions in other field and laboratory studies, though some may be in varying orders of abundance (Akagi et al., 2011; Hatch et al., 2017; Koss et al., 2018; Liu et al., 2017; Müller et al., 2016; Selimovic et al., 2018). For example, Akagi et al. (2011) reported the sum of acetic acid and glycolaldehyde (2.22 g kg^{-1}) essentially equal with formaldehyde as the most abundant VOC from temperate forest fires, similar to FIREX-MFL (2.6 g kg^{-1}) (Selimovic et al., 2018) and WE-CAN (2.4 ± 0.59 g kg^{-1}).

Of important exception, total monoterpenes have been measured in laboratory burns as among the most abundantly emitted VOCs (Akagi et al., 2011; Hatch et al., 2017; Koss et al., 2018). However, they do not rank in the top 30 WE-CAN EFs (0.2 g kg^{-1}), nor the top 10 reported in another aircraft study of western fires (Liu et al., 2017) or one southeastern U.S. prescribed fire (Müller et al., 2016). Akagi et al. (2013) observed large monoterpene emissions from airborne measurements directly over prescribed fires, but also noted that some major monoterpene airborne EFs were significantly lower than those from ground-based samples of the same fires. This may be in part because these monoterpenes tend to be produced from fuels (e.g., dead/down logs) that release emissions with less tendency to be lofted into the main convective column of the plume and sampled by aircraft. Additionally, airborne measurements by larger aircraft such as the NSF/NCAR C-130, may only be possible several minutes downwind of the flame front, thus highly reactive species such as monoterpenes could have undergone some extent of chemical removal before being sampled.

Oxygen-containing VOCs were found to contribute 67% of the tVOC$_{EF}$ (or 61% on a molar basis). It is approximately 5%–10% higher than previous comprehensive laboratory studies of western U.S. fuels (51%–57% of the total on a molar basis; Gilman et al., 2015; Hatch et al., 2017; Koss et al., 2018), potentially reflecting oxidation of VOC emissions before being sampled by the C-130 or differences in the fuel components between studies.
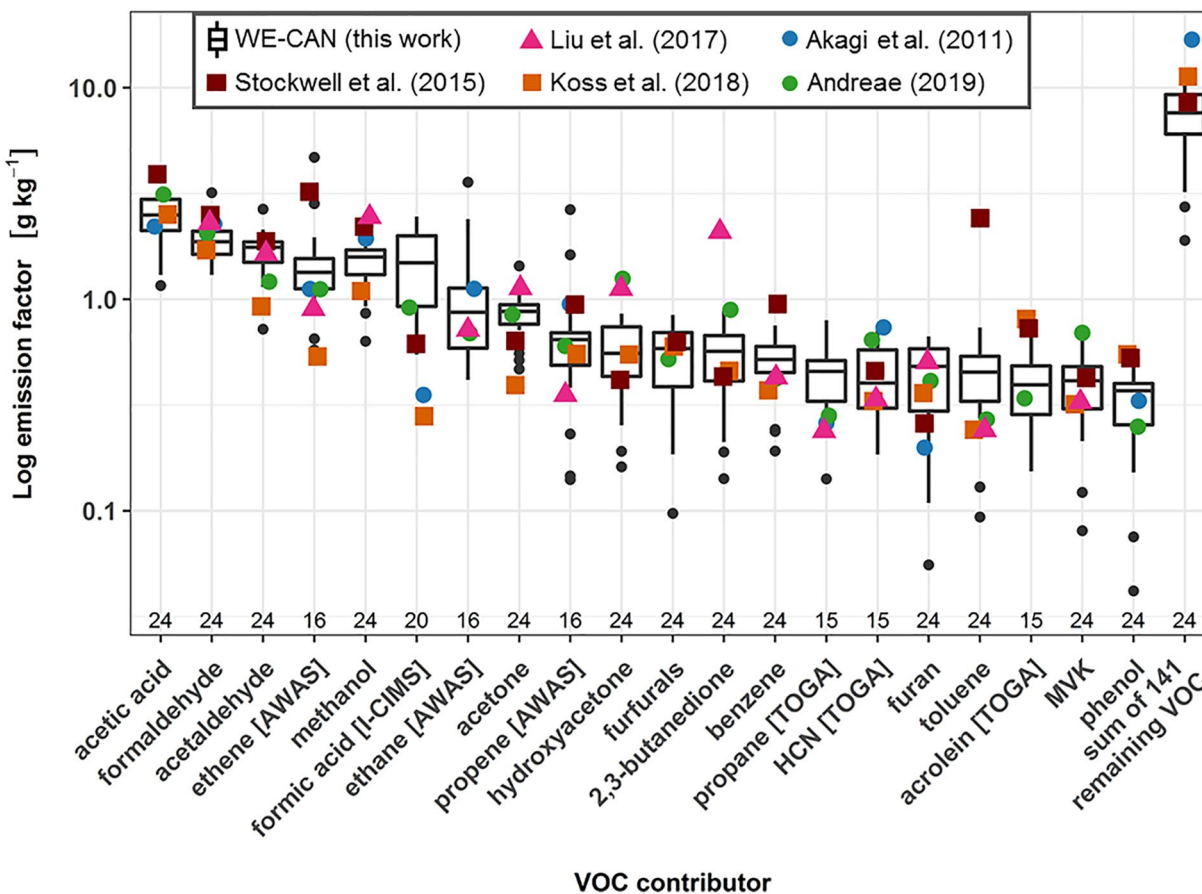
Figure 4. Box plot of emission factors for the 20 most abundantly emitted and remaining VOCs by mass during WE-CAN. The number of "unique fire" EFs (Table 1) used for each box is shown at the bottom of the plot. Also shown are relevant literature values for western U.S. fuel types with round points denoting synthesis studies and squares representing laboratory burns. Specifically, the Akagi et al. (2011) value shown with the "sum of 147 remaining VOC" is the total non-methane organic carbon (NMOC) for temperate forests, excluding the EFs shown for individual VOCs. Andreae (2019) EFs are for temperate forests. The Stockwell et al. (2015) values are the average EFs for relevant western U.S. fuels measured by PTR-ToF-MS and Fourier-transform infrared spectroscopy (FTIR; four black spruce, two juniper, and seven ponderosa pine fueled laboratory burning experiments), weighted by the number of reported burns. The Koss et al. (2018) values are FIREX-MFL western U.S. fuel type study averages, while Liu et al. (2017) report average EFs of three western U.S. wildfires sampled during the Biomass Burning Observation Project (BBOP) and the Studies of Emissions and Atmospheric Composition, Clouds, and Climate Coupling by Regional surveys (SEAC⁴RS) aircraft campaigns. TOGA, AWAS, and I⁻ CIMS measurements are noted in brackets. PTR-ToF-MS measured species names reflect the most abundant isomer at that mass (Koss et al., 2018), and is consistent with the compared literature. Note that $C_2H_4O_2$: acetic acid includes glycolaldehyde, C_3H_6O: acetone includes propanal, $C_3H_6O_2$: hydroxyacetone includes methyl acetate and ethyl formate, $C_5H_4O_2$: furfurals include 2-furfural and 3-furfural, $C_4H_6O_2$: 2,3-butanedione includes methyl acrylate, and C_4H_6O: MVK, MACR includes 2-butenal. Detailed speciation information is available in Table 1.

6. Comparison to Previous Studies

In this section, we compare the WE-CAN campaign-averaged individual EFs to past studies. Five relevant studies were selected: Two PTR-ToF-MS laboratory studies of simulated burns representative of western U.S. fuels (Koss et al., 2018; Stockwell et al., 2015), airborne measurements of wildfire EFs (Liu et al., 2017), a compilation of temperate forest fire EFs based mainly on pine understory prescribed fires (Akagi et al., 2011), and a compilation of >70 field studies of various temperate fuels (Andreae, 2019). Here, we examine differences between field and laboratory measured EFs across individual species in the context of natural fire-to-fire variability and later explore potential explanations for the observed variability in Section 7.

Figure 4 compares WE-CAN EFs for the top 20 most abundantly emitted VOCs (~70% of the measured tVO-C_EF) and the sum of remaining VOCs for the 24 "unique fires" (Table 1). The WE-CAN VOC EFs on a logarithmic scale reveals the large species-to-species and fire-to-fire variability of observed EFs, which except
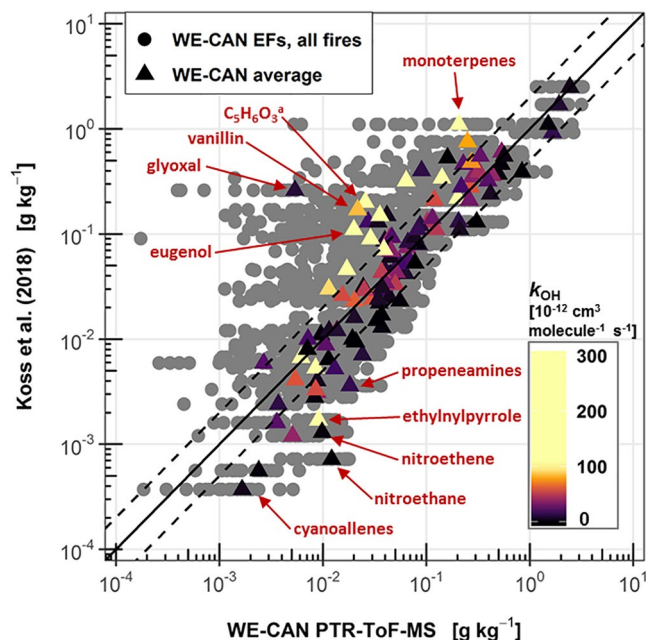
Figure 5. WE-CAN campaign averaged (triangles) and individual fire (gray points) EFs compared to study average EFs reported by Koss et al. (2018) for 116 species measured by PTR-ToF-MS. Campaign averages are colored by each VOC's rate constant for the reaction with OH (k_{OH}) and the scale saturated at 100×10^{12} cm^3 molecules^{-1} s^{-1}. The solid black line represents one-to-one agreement, while the dashed lines represent ± 100%. Additional labels are provided for the five species with the worst agreement when FIREX-MFL average EFs are more than a factor of 2 higher and lower than WE-CAN. [a]5-hydroxymethyl-2[3H]-furanone (Koss et al., 2018).

for formic acid and acrolein, overlap the literature values for similar fuels. Formic acid EFs measured by both I$^-$ CIMS and PTR-ToF-MS (not shown) were higher than the laboratory and synthesis studies, which may be related to the rapid formation in fresh fire plumes (Akagi et al., 2012; Chaliyakunnel et al., 2016; Goode et al., 2000; Pommier et al., 2017; Yokelson et al., 2009). WE-CAN acrolein EFs are consistently lower than in the laboratory, which may reflect chemical loss before airborne sampling. Though WE-CAN EFs largely overlap literature values, there are many individual data points where one or more studies are >1.5 times the interquartile range of the WE-CAN EF, emphasizing the need for multiple biomass burning emission measurements to improve EF statistics.

EFs for many of the VOC species in this work have rarely, if ever, been compared between field and laboratory studies. Figure 5 summarizes how WE-CAN EFs for 116 species measured by PTR-ToF-MS compare to the FIREX-MFL laboratory experiment average (Koss et al., 2018). Reduced major axis regression between the two campaign averages shows overall good agreement with a slope of 0.93 and r^2 of 0.82. Average EFs for 73 species agree within a factor of two between studies. Most species outside of this range when FIREX-MFL EFs are greater than observed during WE-CAN (16 out of 22) have lifetimes <3 h against oxidation by OH (assuming 1×10^6 molec cm^{-3}), such as vanillin, monoterpenes, eugenol, syringol, and sesquiterpenes. This again suggests the potential role of aging and missed emissions from residual smoldering combustion in the field data. Interestingly, in the opposite case when FIREX-MFL average EFs are more than a factor of 2 lower than WE-CAN, 18 out of 21 species are nitrogen-containing VOCs (NVOCs). Recently, NVOC emissions have been associated with low-temperature pyrolysis (Roberts et al., 2020), which is a loose proxy of lower MCE. More NVOC emissions during WE-CAN relative to FIREX-MFL may be due to the lower MCEs observed in the field relative to laboratory burns (Section 7) or fuel nitrogen diffe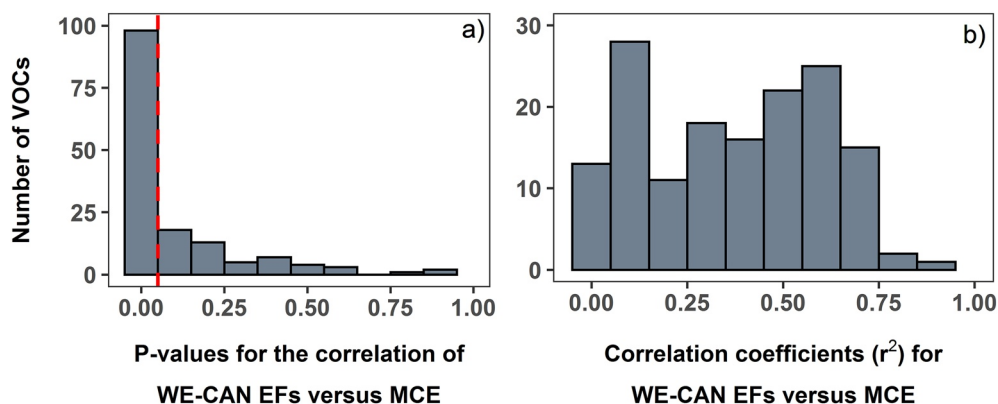rences. Additionally, this could also reflect lager error of PTR-ToF-MS kinetically calculated sensitivities for NVOCs. In Figure 5, the large fire-to-fire variability of WE-CAN measured EFs is again apparent, with many WE-CAN individual fire EFs potentially lower than the FIREX-MFL average.

To quantify the fire-to-fire EF variability, we focus on PTR-ToF-MS (and I$^-$ CIMS) measurements to prevent statistical bias from the smaller TOGA and AWAS sample sizes. Of these, the median fire-to-fire EF coefficient of variation (COV, standard deviation divided by the mean) is 43% (45% mean; Table 2). Nitromethane, formaldehyde, isocyanic acid, and acetic acid have the least variable EFs with COVs of 11%–25% for the campaign and ranges varying by less than a factor of 3. Conversely, the most variable species are some of the most reactive (monoterpenes, creosol, vanillin, and sesquiterpenes; COV 73%–108%), suggesting a potential role of rapid early plume chemistry in the observed variability. The "sum of remaining VOCs" further characterizes the variability, ranging by nearly a factor of 4 across all fires with 29% COV (a factor of 2 and 23% COV on a molar basis).

7. Dependence of Emission Factors on the Modified Combustion Efficiency

Though direct comparisons of campaign averaged EFs as in Figures 4 and 5 are common in the literature for showing agreement between studies, such comparisons largely ignore the dependence of EFs on combustion processes. In this section, we explore the relationship between MCE and EFs for all measured VOCs in an attempt to explain some of the observed variability and relate WE-CAN observations to the growing EF literature with the simple combustion proxy that is readily measured in the field.

Figure 6. (a) Histogram of p-values from the least squares regression of EF versus MCE for 151 VOCs. Among them, 98 VOC EFs have a statistically significant correlation with MCE, *p*-values <0.05, represented by the red dashed line. (b) The same as panel (a) except for correlation coefficients (r^2) of the least squares regression of EF versus MCE.

7.1. Individual VOC Emission

Figure 6 shows that 98 out of 151 reported VOC EFs, measured in at least 10 of the 24 fires, correlate to MCE with *p*-values <0.05, indicating that 76% of the average $tVOC_{EF}$ has statistically significant dependence on burning conditions. Of these, correlation coefficients range from 0.23 for quinone to 0.91 for benzene and all slopes are negative. The wide range of correlation coefficients suggests MCE is not the only contributor to the emission variability, with fuel types/conditions (decomposition, elemental chemistry, geometry, and moisture), plume aging, surface wind, and pyrolysis temperature likely playing a role (Roberts et al., 2020; Sekimoto et al., 2018). Still, the correlations obtained by WE-CAN can provide observational constraints on uncertainties for predicting VOC emissions with MCE, particularly for those species that are rarely measured in the field. Overall, we find that MCE can explain at least 50% of the variance for 57 individual VOC EFs, representing 54% of the $tVOC_{EF}$. Equations and coefficients for these 151 correlations are listed in the supplement (Table S5).

We compare WE-CAN EFs to previous studies in terms of their dependence on MCE for CH_4 and five VOCs selected for their representativeness as discussed below. Figure 7 shows that when MCE is considered, WE-CAN EFs show good agreement with both laboratory and field measurements, with a slightly better agreement with field data. This may reflect chemical aging effects or under-representation of emissions from residual smoldering combustion in the field relative to the laboratory. Benzene, methanol, and CH_4 represent long-lived species with minimal degradation in the plume aging times characteristic of the WE-CAN emission transects. Interestingly, the spread in the laboratory benzene EFs is larger than the field data, the reason for which is currently unknown. Furan represents shorter-lived species, while acetaldehyde and formaldehyde are a photochemical product of many VOCs. Finally, the figure highlights the agreement between EFs as a function of MCE for CH_4 measurements obtained by the NCAR Picarro instrument and literature values. A few notable outliers are also present. The outlying point from Stockwell et al. (2015) represents a ponderosa pine lab burn. Furan's outlier is from combustion of Jeffrey pine duff (Koss et al., 2018), and is also present in the comparison of furfural EFs versus MCE (Figure S4).

Although the comparison of these six species is not inherently representative of the other 156 VOCs reported in this work, they do suggest that WE-CAN measured EFs agree with previous studies when compared in the context of MCE. Additionally, Figure 7 highlights that despite complex fuels and combustion chemistry, the simple MCE index explains a significant amount of the study-to-study variability. The remaining variance is expected due to fuel chemistry, moisture, geometry, or measurement uncertainty (Yokelson et al., 1996), and should be further explored as more field data becomes available.
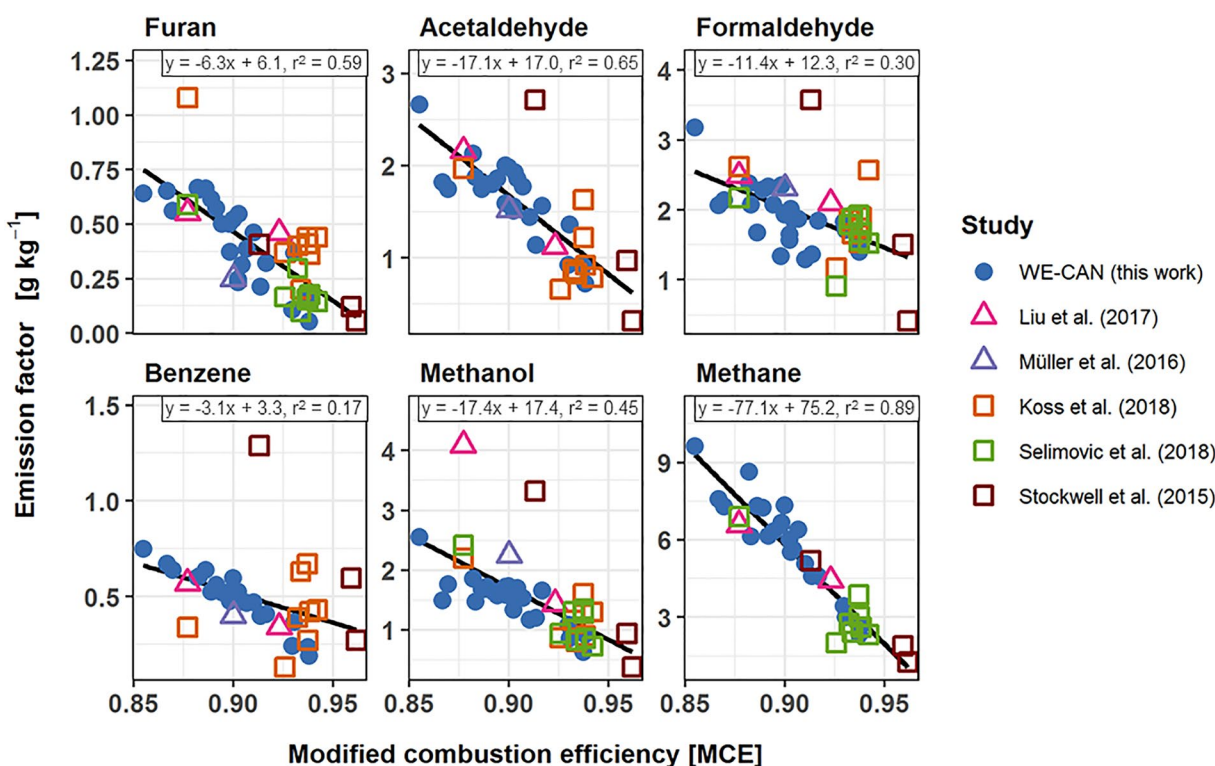
Figure 7. Correlations of EFs versus MCE for methane and a subset of VOCs (furan, acetaldehyde, formaldehyde, benzene, and methanol) commonly reported in the literature. Also shown are additional EFs for two field campaigns (Liu et al., 2017; Müller et al., 2016) and averaged coniferous fuel EFs measured during three laboratory burn experiments (Koss et al., 2018; Selimovic et al., 2018; Stockwell et al., 2015). We also show the same figure for furfurals in Figure S4 as an additional short lived VOC. Black lines represent the least squares regression for all studies. Regression statistics of all 151 VOC EFs with MCE measured in at least 10 fires during WE-CAN are available in Table S5.

7.2. Total Measured VOC Emissions

WE-CAN total measured VOC emissions strongly correlate with MCE ($r^2 = 0.67$; Figure 8), indicative of less VOC being produced relative to CO_2 as fuels burn more efficiently and that nearly 70% of the $tVOC_{EF}$ can be explained by MCE alone. Total measured VOC emissions for western U.S. fuels measured during combined laboratory burns also show a strong negative correlation with MCE ($r^2 = 0.72$), however with a much steeper slope and approximately two times greater $tVOC_{EF}$ than WE-CAN at similar MCEs. Overall, such strong correlations observed both in the field and laboratory studies suggest that total measured VOC emissions could be predicted when the MCE information is available, and individual VOC emission could be subsequently derived using emission profiles (Section 8), similar to the wildland fire portion of the EPA's National Emission Inventory (Baker et al., 2016; U.S. Environmental Protection Agency, 2020)

There are a few potential reasons for the differences between the WE-CAN and laboratory $tVOC_{EF}$. First, rapid chemistry taking place in the wildfire plumes before their sampling by the C-130 could result in lower EFs compared to laboratory studies particularly for shorter-lived species, which also tend to have high molecular weights. Similarly, condensation of lower volatility species between emission and sampling may also account for some of the mass difference. Ground-based studies of wildfire $\Delta PM_{2.5}/\Delta CO$ ratios show that considerable evaporation of biomass burning organic aerosol occurs at the warmer temperatures typical of ground-level and laboratory burn environments relative to aircraft sampling (Selimovic et al., 2019). Including the WE-CAN average OA ($\sim$19 g kg^{-1}) in the $tVOC_{EF}$ would help achieve agreement, but not all OA evaporates at room temperature so this does not fully resolve the differences between studies. Second, a forced flow directly to the sample inlets during laboratory burns likely means that they capture some emissions from smoldering combustion which may not be as efficiently lofted in the wildfire plume and thus underreported in the field. Third, in this work we assume 45.7% emitted carbon in our carbon mass balance for deriving EFs following other field studies in the western U.S., which contrasts with the $\sim$50%
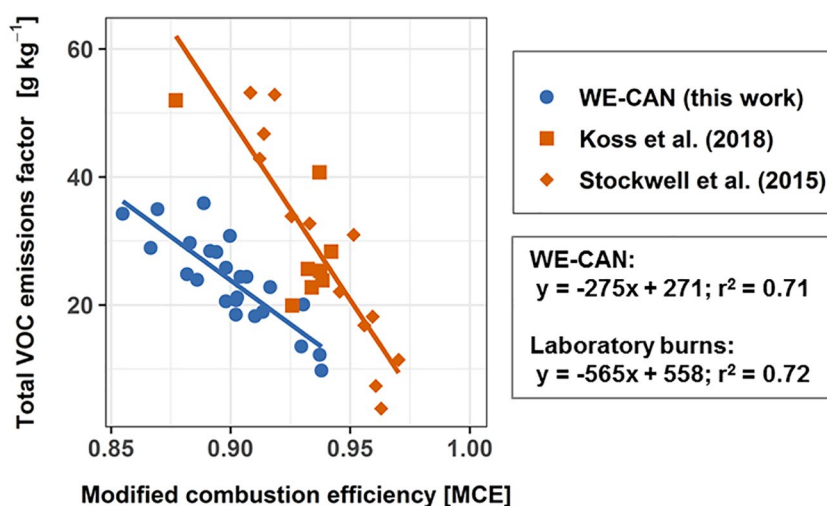
Figure 8. Relationship between total measured VOC emissions and MCE observed in WE-CAN. Also shown are data from laboratory burns for similar fuels during FLAME-4 and FIREX-MFL. The solid lines are corresponding least squares regression fits. WE-CAN total measured VOC emissions include the 161 VOC EFs reported in this study. Koss et al. (2018) total VOC include ~154 PTR-ToF-MS measured ions, excluding ammonia and nitrous acid, from individual burns of ponderosa pine, lodgepole pine, Douglas fir, subalpine fir, Engelmann spruce, loblolly pine, Jeffrey pine, and juniper fuel types. Stockwell et al. (2015) total measured VOC emissions include ~55 PTR-ToF-MS measured ions reported as positively identified and 10 VOCs measured by Fourier-transform infrared spectroscopy (FTIR) during four black spruce, two juniper, and seven ponderosa pine fueled laboratory burning experiments.

used during the laboratory studies (Koss et al., 2018; Stockwell et al., 2015), meaning WE-CAN EFs are generally expected to be ~10% lower (Equation 3). Additionally, WE-CAN EFs were calculated using the sum of carbon from 161 ions and individual VOCs, along with OA, BC, CO, CO_2, and CH_4 for the total carbon term of the mass balance equation (Equation 3), which is expected to result in slightly lower individual EFs than if a smaller sampling of VOCs, CO, CO_2, and CH_4 are only used. Finally, the data available to calculate MCE differs substantially between laboratory and field experiments. In the lab, the full progression of a fire from ignition to completion is measured, and MCE is therefore calculated using the fire integrated CO and CO_2 measurements, providing the fire's overall MCE for the entirety of the burn. While this includes both flaming and smoldering time periods, the laboratory integrated MCE remains higher than in the field due to a number of factors including drier fuels and more optimal burning conditions (Christian et al., 2003; Holder et al., 2017; Selimovic et al., 2018; Yokelson et al., 2013). In the field, MCE is calculated from a single transect through a smoke plume which is assumed to contain all the stages of burning. It is likely a combination of the above factors contributes to the difference in $tVOC_{EF}$ versus MCE between field data and laboratory burns. While we cannot ascertain the exact reasons for lab field differences, the comparison highlights the importance of field measurements of authentic fires.

Rapid early plume chemistry can cause aircraft-measured EFs of reactive primary VOCs to be lower than at the source, while simultaneously increasing EFs for secondary species. Field and laboratory measured MCEs also differ, making the decision of which EFs to use in models unclear. Generally, laboratory burns may better capture the emissions and evolution of reactive VOCs throughout fires, including smoldering combustion, or provide an opportunity to control variables. However, WE-CAN sampled western U.S. wildfires mid-afternoon during the summer, when presumably the fires are burning at their highest emissions production level. Within this data set, only 4 out of the 24 "unique fires" were characterized by MCE > 0.92, which is near the lower end of MCEs typically reported for laboratory burns of similar fuels. Airborne measurements would be expected to favor flaming combustion if they have a bias, so a lower MCE in the air suggests a tendency toward unrepresentative high MCE in many lab burns. For this reason, many laboratory studies provide EFs adjusted to reflect the field average MCE (Selimovic et al., 2018). Interestingly, aging effects may change the airborne EFs to levels that are perhaps more appropriate for the spatial and temporal resolution of many regions to global models (Lonsdale et al., 2020), but it is not simple to rule out the loss of smoldering emissions in airborne sampled fires (Akagi et al., 2014; Bertschi et al., 2003). Overall, using data

from real wildfires makes sense, but lab studies can help characterize species rarely or not measured in the field, especially if they are adjusted to match field MCE or other steps are taken to increase representativeness (Selimovic et al., 2018; Yokelson et al., 2013).

8. VOC Emission Profiles for Emissions Speciation

Rather than using correlations with MCE to predict individual VOC EF, another approach to get speciated emissions is by applying a flaming or smoldering profile to the total VOC emissions (U.S. Environmental Protection Agency, 2020). Here, we calculate VOC emission profiles by dividing individual VOC EFs by the tVOC$_{EF}$ to get the mass fraction of each species to the total emissions. Mass fractions for the five highest and five lowest MCE fires sampled during WE-CAN were then binned into a "high" and "low" MCE profile. A Wilcox rank-sum test comparing the two profiles shows that only 26 VOCs, ~18% of the tVOC$_{EF}$, are statistically different between the profiles (p-values < 0.05); among them, only 3 VOCs (methylpyridines, isocyanic acid, and toluene) have p-values < 0.01. This suggests that for the majority of VOCs ($>80\%$ by mass) emitted in western U.S. wildfires, mass fractions of individual VOCs significantly overlap for the MCE range sampled during WE-CAN. As such, separated high and low MCE profiles cannot be clearly defined here and a single campaign averaged VOC emission profile best describes the data for all but a few species (Table 2).

To examine the role of MCE on emission profiles, we further investigate the dependence of the mass fraction on MCE for the same 151 species, measured in 10 or more fires, as in Section 7.1. In contrast to EF versus MCE correlations, we find that the mass fractions of only 44 of the 151 species have a statistically significant dependence on MCE (p-values < 0.05) with correlation coefficients ranging from 0.17 to 0.62. These 44 VOCs account for 31% of the average tVOC$_{EF}$. Additionally, 11 of these correlations have positive slopes, with three of the steepest being for formic acid, formaldehyde, and isocyanic acid, indicating that these VOCs account for more of the tVOC$_{EF}$ as combustion efficiency increases.

Recently it has been shown that laboratory biomass burning VOC emissions could be described by two positive matrix factorization (PMF) factors related to high-temperature and low-temperature pyrolysis, where pyrolysis is one component of smoldering combustion (Sekimoto et al., 2018). One possible explanation for the lack of distinct high and low MCE emission profiles in this study is that emissions from all types of burning (including flaming, gasification, and high-temperature and low-temperature pyrolysis) are lofted into the large wildfire plumes sampled during WE-CAN, which likely results in the high and low MCE emissions intermixing such that the measured VOC profile regresses toward a mean. This is in contrast to laboratory burns where both "pure" and mixed combustion processes can be observed as the burn progresses from ignition to completion. Consequently, these results may be different if airborne data are obtained over a broader range of MCEs, such that similar direct comparison between smoldering and flaming emissions can be done.

9. Conclusions

We present EFs and ERs for 161 isomeric and individual VOCs for western U.S. wildfires measured by complementary instruments onboard the NSF/NCAR C-130 aircraft during the WE-CAN field campaign. In situ emission measurements were made during 31 emission transects of 24 "unique" wildfires, significantly expanding the number of observations of many VOCs rarely reported in the field and allowing us to assess the large natural variability of wildfire emissions. Across all fires, measured MCEs ranged from 0.85 to 0.94 when they were typically burning most actively in the mid-to-late afternoon.

Using co-deployed TOGA measurements for 13 speciated VOCs, we found that the fractional contribution of isomers to four PTR-ToF-MS measured ions (m/z 59.049, 71.049, 107.086, and 137.132) had relatively little fire-to-fire variability and were comparable to results in previous laboratory burn experiments for similar fuels. Among 45 co-measured VOCs, 36 showed agreement within combined instrument uncertainties ($<60\%$). Disagreement was found between five PTR-ToF-MS ion masses and the two GC-based measurements (m/z 69.070 isoprene, m/z 69.033 furan, m/z 83.049 methylfurans, m/z 121.061 C$_9$ aromatics, and m/z 137.132 monoterpenes), likely reflecting additional unknown isomers or fragment products detected by PTR-ToF-MS in fire smoke. Given that these ions represent several reactive VOCs, their further

identification could help improve PTR-ToF-MS measurements and better understand their implications for air quality. TOGA and AWAS measurements agree between all co-measured species with the exception of 3-methylpentane.

The total observed VOC emissions averaged 26.1 ± 6.9 g kg^{-1} (148.3 ± 29.6 ppbv ppmv^{-1}) for western U.S. wildfires, consistent with previous studies. The top 10 most abundant VOCs accounted for 53% of the total measured VOC mass; while the remaining 47% was represented by at least 151 species, each contributing less than 2% to the total. Oxygenated VOCs contributed to 67% of the measured total VOC emissions by mass, or 61% on a molar basis.

When MCE is considered, we found overall good agreement between individual VOC EFs and previous laboratory and field studies. However, for a given MCE, total measured VOC emissions are nearly two times lower than measured in two recent laboratory experiments utilizing similar instrumentation and nominally similar fuels. The source of this difference may reflect aging effects, fuel differences, under-sampling of smoldering emissions by aircraft, or different integration of combustion processes. WE-CAN observations reveal 98 species, accounting for 76% of the average total measured VOC mass, have statistically significant and negative dependences on MCE. VOC mass fractions show much less MCE dependence with significant overlap within the observed MCE range, suggesting that a single speciation profile can describe VOC emissions for the western U.S. coniferous forest wildfires sampled during WE-CAN.

Overall, WE-CAN field observations nearly double the number of measured VOC ERs and EFs for wildfires compared to the most recent synthesis study, and double the number of western U.S. airborne samples for near-field fire emissions, providing better constraints for air quality models. However, plane safety and logistical concerns limited WE-CAN measurements to sampling plumes mid-to-late afternoon and tens of minutes downwind of a fire. Future studies of wildfire emissions from the less active (and possibly lower MCE) burning conditions typical of nighttime and early morning would complement the WE-CAN data set. Additionally, more work connecting ground-based studies to laboratory and aircraft observations would better inform how smoldering combustion emissions, not lofted into the main plume, may bias airborne measurements. Finally, future model and observational plume aging studies are needed to improve our understanding of how rapid early plume chemistry in wildfires may impact comparisons between laboratory and field-measured EFs for reactive VOCs and the total organic emissions.

Data Availability Statement

The data were collected using NSF's Lower Atmosphere Observing Facilities, which are managed and operated by NCAR's Earth Observing Laboratory. All data are available in the WE-CAN data archive (https://data.eol.ucar.edu/master_lists/generated/we-can/; Merge version R3 is used in this study).

References

Akagi, S. K., Burling, I. R., Mendoza, A., Johnson, T. J., Cameron, M., Griffith, D. W. T., et al. (2014). Field measurements of trace gases emitted by prescribed fires in southeastern US pine forests using an open-path FTIR system. *Atmospheric Chemistry and Physics*, *14*(1), 199–215. https://doi.org/10.5194/acp-14-199-2014

Akagi, S. K., Craven, J. S., Taylor, J. W., McMeeking, G. R., Yokelson, R. J., Burling, I. R., et al. (2012). Evolution of trace gases and particles emitted by a chaparral fire in California. *Atmospheric Chemistry and Physics*, *12*(3), 1397–1421. https://doi.org/10.5194/acp-12-1397-2012

Akagi, S. K., Yokelson, R. J., Burling, I. R., Meinardi, S., Simpson, I., Blake, D. R., et al. (2013). Measurements of reactive trace gases and variable O_3 formation rates in some South Carolina biomass burning plumes. *Atmospheric Chemistry and Physics*, *13*(3), 1141–1165. https://doi.org/10.5194/acp-13-1141-2013

Akagi, S. K., Yokelson, R. J., Wiedinmyer, C., Alvarado, M. J., Reid, J. S., Karl, T., et al. (2011). Emission factors for open and domestic biomass burning for use in atmospheric models. *Atmospheric Chemistry and Physics*, *11*(9), 4039–4072. https://doi.org/10.5194/acp-11-4039-2011

Andreae, M. O. (2019). Emission of trace gases and aerosols from biomass burning – An updated assessment. *Atmospheric Chemistry and Physics*, *19*(13), 8523–8546. https://doi.org/10.5194/acp-19-8523-2019

Andreae, M. O., & Merlet, P. (2001). Emission of trace gases and aerosols from biomass burning. *Global Biogeochemical Cycles*, *15*(4), 955–966. https://doi.org/10.1029/2000GB001382

Andrews, S. J., Carpenter, L. J., Apel, E. C., Atlas, E., Donets, V., Hopkins, J. R., et al. (2016). A comparison of very short lived halocarbon (VSLS) and DMS aircraft measurements in the tropical west Pacific from CAST, ATTREX and CONTRAST. *Atmospheric Measurement Techniques*, *9*(10), 5213–5225. https://doi.org/10.5194/amt-9-5213-2016

Apel, E. C., Emmons, L. K., Karl, T., Flocke, F., Hills, A. J., Madronich, S., et al. (2010). Chemical evolution of volatile organic compounds in the outflow of the Mexico City Metropolitan area. *Atmospheric Chemistry and Physics*, *10*(5), 2353–2375. https://doi.org/10.5194/acp-10-2353-2010

Apel, E. C., Hills, A. J., Lueb, R., Zindel, S., Eisele, S., & Riemer, D. D. (2003). A fast-GC/MS system to measure C_2 to C_4 carbonyls and methanol aboard aircraft. *Journal of Geophysical Research: Atmospheres*, *108*(D20), 8794. https://doi.org/10.1029/2002JD003199

Apel, E. C., Hornbrook, R. S., Hills, A. J., Blake, N. J., Barth, M. C., Weinheimer, A., et al. (2015). Upper tropospheric ozone production from lightning NOx-impacted convection: Smoke ingestion case study from the DC3 campaign. *Journal of Geophysical Research: Atmospheres*, *120*(6), 2505–2523. https://doi.org/10.1002/2014JD022121

Baasandorj, M., Millet, D. B., Hu, L., Mitroo, D., & Williams, B. J. (2015). Measuring acetic and formic acid by proton-transfer-reaction mass spectrometry: Sensitivity, humidity dependence, and quantifying interferences. *Atmospheric Measurement Techniques*, *8*(3), 1303–1321. https://doi.org/10.5194/amt-8-1303-2015

Baker, K. R., Woody, M. C., Tonnesen, G. S., Hutzell, W., Pye, H. O. T., Beaver, M. R., et al. (2016). Contribution of regional-scale fire events to ozone and PM2.5 air quality estimated by photochemical modeling approaches. *Atmospheric Environment*, *140*, 539–554. https://doi.org/10.1016/j.atmosenv.2016.06.032

Benedict, K. B., Prenni, A. J., El-Sayed, M. M. H., Hecobian, A., Zhou, Y., Gebhart, K. A., et al. (2020). Volatile organic compounds and ozone at four national parks in the southwestern United States. *Atmospheric Environment*, *239*, 117783. https://doi.org/10.1016/j.atmosenv.2020.117783

Benedict, K. B., Zhou, Y., Sive, B. C., Prenni, A. J., Gebhart, K. A., Fischer, E. V., et al. (2019). Volatile organic compounds and ozone in Rocky Mountain National Park during FRAPPÉ. *Atmospheric Chemistry and Physics*, *19*(1), 499–521. https://doi.org/10.5194/acp-19-499-2019

Bertschi, I., Yokelson, R. J., Ward, D. E., Babbitt, R. E., Susott, R. A., Goode, J. G., & Hao, W. M. (2003). Trace gas and particle emissions from fires in large diameter and belowground biomass fuels. *Journal of Geophysical Research*, *108*(D13), 8472. https://doi.org/10.1029/2002JD002100

Bowman, D. M. J. S., Williamson, G. J., Abatzoglou, J. T., Kolden, C. A., Cochrane, M. A., & Smith, A. M. S. (2017). Human exposure and sensitivity to globally extreme wildfire events. *Nature Ecology and Evolution*, *1*(3), 0058. https://doi.org/10.1038/s41559-016-0058

Bruns, E. A., Slowik, J. G., El Haddad, I., Kilic, D., Klein, F., Dommen, J., et al. (2017). Characterization of gas-phase organics using proton transfer reaction time-of-flight mass spectrometry: Fresh and aged residential wood combustion emissions. *Atmospheric Chemistry and Physics*, *17*(1), 705–720. https://doi.org/10.5194/acp-17-705-2017

Canagaratna, M. R., Jimenez, J. L., Kroll, J. H., Chen, Q., Kessler, S. H., Massoli, P., et al. (2015). Elemental ratio measurements of organic compounds using aerosol mass spectrometry: Characterization, improved calibration, and implications. *Atmospheric Chemistry and Physics*, *15*(1), 253–272. https://doi.org/10.5194/acp-15-253-2015

Carter, T. S., Heald, C. L., Jimenez, J. L., Campuzano-Jost, P., Kondo, Y., Moteki, N., et al. (2020). How emissions uncertainty influences the distribution and radiative impacts of smoke from fires in North America. *Atmospheric Chemistry and Physics*, *20*(4), 2073–2097. https://doi.org/10.5194/acp-20-2073-2020

Chaliyakunnel, S., Millet, D. B., Wells, K. C., Cady-Pereira, K. E., & Shephard, M. W. (2016). A large underestimate of formic acid from tropical fires: Constraints from space-borne measurements. *Environmental Science & Technology*, *50*(11), 5631–5640. https://doi.org/10.1021/acs.est.5b06385

Christian, T. J., Kleiss, B., Yokelson, R. J., Holzinger, R., Crutzen, P. J., Hao, W. M., et al. (2003). Comprehensive laboratory measurements of biomass-burning emissions: 1. Emissions from Indonesian, African, and other fuels. *Journal of Geophysical Research*, *108*(D23), 4719. https://doi.org/10.1029/2003JD003704

Coggon, M. M., Lim, C. Y., Koss, A. R., Sekimoto, K., Yuan, B., Gilman, J. B., et al. (2019). OH chemistry of non-methane organic gases (NMOGs) emitted from laboratory and ambient biomass burning smoke: evaluating the influence of furans and oxygenated aromatics on ozone and secondary NMOG formation. *Atmospheric Chemistry and Physics*, *19*(23), 14875–14899. https://doi.org/10.5194/acp-19-14875-2019

Crutzen, P. J., & Andreae, M. O. (1990). Biomass burning in the tropics: Impact on atmospheric chemistry and biogeochemical cycles. *Science*, *250*(4988), 1669–1678. https://doi.org/10.1126/science.250.4988.1669

de Gouw, J. A., Goldan, P. D., Warneke, C., Kuster, W. C., Roberts, J. M., Marchewka, M., et al. (2003). Validation of proton transfer reaction-mass spectrometry (PTR-MS) measurements of gas-phase organic compounds in the atmosphere during the New England Air Quality Study (NEAQS) in 2002. *Journal of Geophysical Research*, *108*(D21), 4682. https://doi.org/10.1029/2003JD003863

Ferek, R. J., Reid, J. S., Hobbs, P. V., Blake, D. R., & Liousse, C. (1998). Emission factors of hydrocarbons, halocarbons, trace gases and particles from biomass burning in Brazil. *Journal of Geophysical Research*, *103*(D24), 32107–32118. https://doi.org/10.1029/98JD00692

Friedli, H. R., Atlas, E., Stroud, V. R., Giovanni, L., Campos, T., & Radke, L. F. (2001). Volatile organic trace gases emitted from North American wildfires. *Global Biogeochemical Cycles*, *15*(2), 435–452. https://doi.org/10.1029/2000GB001328

Garofalo, L. A., Pothier, M. A., Levin, E. J. T., Campos, T., Kreidenweis, S. M., & Farmer, D. K. (2019). Emission and evolution of submicron organic aerosol in smoke from wildfires in the western United States. *ACS Earth and Space Chemistry*, *3*(7), 1237–1247. https://doi.org/10.1021/acsearthspacechem.9b00125

Gilman, J. B., Lerner, B. M., Kuster, W. C., Goldan, P. D., Warneke, C., Veres, P. R., et al. (2015). Biomass burning emissions and potential air quality impacts of volatile organic compounds and other trace gases from fuels common in the US. *Atmospheric Chemistry and Physics*, *15*(24), 13915–13938. https://doi.org/10.5194/acp-15-13915-2015

Goode, J. G., Yokelson, R. J., Ward, D. E., Susott, R. A., Babbitt, R. E., Davies, M. A., & Hao, W. M. (2000). Measurements of excess O_3, CO_2, CO, CH_4, C_2H_4, C_2H_2, HCN, NO, NH_3, HCOOH, CH_3COOH, HCHO, and CH_3OH in 1997 Alaskan biomass burning plumes by airborne Fourier transform infrared spectroscopy (AFTIR). *Journal of Geophysical Research*, *105*(D17), 22147–22166. https://doi.org/10.1029/2000JD900287

Gueneron, M., Erickson, M. H., VanderSchelden, G. S., & Jobson, B. T. (2015). PTR-MS fragmentation patterns of gasoline hydrocarbons. *International Journal of Mass Spectrometry*, *379*, 97–109. https://doi.org/10.1016/j.ijms.2015.01.001

Guérette, E.-A., Paton-Walsh, C., Desservettaz, M., Smith, T. E. L., Volkova, L., Weston, C. J., & Meyer, C. P. (2018). Emissions of trace gases from Australian temperate forest fires: Emission factors and dependence on modified combustion efficiency. *Atmospheric Chemistry and Physics*, *18*(5), 3717–3735. https://doi.org/10.5194/acp-18-3717-2018

Haase, K. B., Keene, W. C., Pszenny, A. A. P., Mayne, H. R., Talbot, R. W., & Sive, B. C. (2012). Calibration and intercomparison of acetic acid measurements using proton-transfer-reaction mass spectrometry (PTR-MS). *Atmospheric Measurement Techniques*, *5*(11), 2739–2750. https://doi.org/10.5194/amt-5-2739-2012

Hatch, L. E., Jen, C. N., Kreisberg, N. M., Selimovic, V., Yokelson, R. J., Stamatis, C., et al. (2019). Highly speciated measurements of terpenoids emitted from laboratory and mixed-conifer forest prescribed fires. *Environmental Science & Technology*, *53*(16), 9418–9428. https://doi.org/10.1021/acs.est.9b02612

Hatch, L. E., Yokelson, R. J., Stockwell, C. E., Veres, P. R., Simpson, I. J., Blake, D. R., et al. (2017). Multi-instrument comparison and compilation of non-methane organic gas emissions from biomass burning and implications for smoke-derived secondary organic aerosol precursors. *Atmospheric Chemistry and Physics*, *17*(2), 1471–1489. https://doi.org/10.5194/acp-17-1471-2017

Hobbs, P. V., Sinha, P., Yokelson, R. J., Christian, T. J., Blake, D. R., Gao, S., et al. (2003). Evolution of gases and particles from a savanna fire in South Africa. *Journal of Geophysical Research*, *108*(D13), 8485. https://doi.org/10.1029/2002JD002352

Holder, A. L., Gullett, B. K., Urbanski, S. P., Elleman, R., O'Neill, S., Tabor, D., et al. (2017). Emissions from prescribed burning of agricultural fields in the Pacific Northwest. *Atmospheric Environment*, *166*, 22–33. https://doi.org/10.1016/j.atmosenv.2017.06.043

Hornbrook, R. S., Blake, D. R., Diskin, G. S., Fried, A., Fuelberg, H. E., Meinardi, S., et al. (2011). Observations of nonmethane organic compounds during ARCTAS − Part 1: Biomass burning emissions and plume enhancements. *Atmospheric Chemistry and Physics*, *11*(21), 11103–11130. https://doi.org/10.5194/acp-11-11103-2011

Jaffe, D. A., O'Neill, S. M., Larkin, N. K., Holder, A. L., Peterson, D. L., Halofsky, J. E., & Rappold, A. G. (2020). Wildfire and prescribed burning impacts on air quality in the United States. *Journal of the Air & Waste Management Association*, *70*(6), 583–615. https://doi.org/10.1080/10962247.2020.1749731

Jolly, W. M., Cochrane, M. A., Freeborn, P. H., Holden, Z. A., Brown, T. J., Williamson, G. J., & Bowman, D. M. J. S. (2015). Climate-induced variations in global wildfire danger from 1979 to 2013. *Nature Communications*, *6*, 7537. https://doi.org/10.1038/ncomms8537

Juncosa Calahorrano, J. F., Lindaas, J., O'Dell, K., Palm, B. B., Peng, Q., Flocke, F., et al. (2021). Daytime oxidized reactive nitrogen partitioning in western U.S. wildfire smoke plumes. *Journal of Geophysical Research: Atmospheres*, *126*(4), e2020JD033484. https://doi.org/10.1029/2020JD033484

Kaiser, J. W., Heil, A., Andreae, M. O., Benedetti, A., Chubarova, N., Jones, L., et al. (2012). Biomass burning emissions estimated with a global fire assimilation system based on observed fire radiative power. *Biogeosciences*, *9*(1), 527–554. https://doi.org/10.5194/bg-9-527-2012

Karl, T., Hansel, A., Cappellin, L., Kaser, L., Herdlinger-Blatt, I., & Jud, W. (2012). Selective measurements of isoprene and 2-methyl-3-buten-2-ol based on NO^+ ionization mass spectrometry. *Atmospheric Chemistry and Physics*, *12*(24), 11877–11884. https://doi.org/10.5194/acp-12-11877-201

Koss, A. R., Sekimoto, K., Gilman, J. B., Selimovic, V., Coggon, M. M., Zarzana, K. J., et al. (2018). Non-methane organic gas emissions from biomass burning: Identification, quantification, and emission factors from PTR-ToF during the FIREX 2016 laboratory experiment. *Atmospheric Chemistry and Physics*, *18*(5), 3299–3319. https://doi.org/10.5194/acp-18-3299-2018

Larkin, N. K., Raffuse, S. M., & Strand, T. M. (2014). Wildland fire emissions, carbon, and climate: U.S. emissions inventories. *Forest Ecology and Management*, *317*, 61–69. https://doi.org/10.1016/j.foreco.2013.09.012

Lee, B. H., Lopez-Hilfiker, F. D., Mohr, C., Kurtén, T., Worsnop, D. R., & Thornton, J. A. (2014). An iodide-adduct high-resolution time-of-flight chemical-ionization mass spectrometer: Application to atmospheric inorganic and organic compounds. *Environmental Science & Technology*, *48*(11), 6309–6317. https://doi.org/10.1021/es500362a

Lindaas, J., Pollack, I. B., Garofalo, L. A., Pothier, M. A., Farmer, D. K., Kreidenweis, S. M., et al. (2021). Emissions of reactive nitrogen from western U.S. wildfires during summer 2018. *Journal of Geophysical Research: Atmospheres*, *126*(2). e2020JD032657. https://doi.org/10.1029/2020JD032657

Liu, X., Huey, L. G., Yokelson, R. J., Selimovic, V., Simpson, I. J., Müller, M., et al. (2017). Airborne measurements of western U.S. wildfire emissions: Comparison with prescribed burning and air quality implications. *Journal of Geophysical Research: Atmospheres*, *122*(11), 6108–6129. https://doi.org/10.1002/2016JD026315

Lonsdale, C. R., Alvarado, M. J., Hodshire, A. L., Ramnarine, E., & Pierce, J. R. (2020). Simulating the forest fire plume dispersion, chemistry, and aerosol formation using SAM-ASP version 1.0. *Geoscientific Model Development*, *13*(9), 4579–4593. https://doi.org/10.5194/gmd-13-4579-2020

McClure, C. D., & Jaffe, D. A. (2018). US particulate matter air quality improves except in wildfire-prone areas. *Proceedings of the National Academy of Sciences of the United States of America*, *115*(31), 7901–7906. https://doi.org/10.1073/pnas.1804353115

Müller, M., Anderson, B. E., Beyersdorf, A. J., Crawford, J. H., Diskin, G. S., Eichler, P., et al. (2016). In situ measurements and modeling of reactive trace gases in a small biomass burning plume. *Atmospheric Chemistry and Physics*, *16*(6), 3813–3824. https://doi.org/10.5194/acp-16-3813-2016

O'Dell, K., Ford, B., Fischer, E. V., & Pierce, J. R. (2019). Contribution of wildland-fire smoke to US PM2.5 and its influence on recent trends. *Environmental Science & Technology*, *53*(4), 1797–1804. https://doi.org/10.1021/acs.est.8b05430

Ottmar, R. D. (2014). Wildland fire emissions, carbon, and climate: Modeling fuel consumption. *Forest Ecology and Management*, *317*, 41–50. https://doi.org/10.1016/j.foreco.2013.06.010

Pagonis, D., Sekimoto, K., & de Gouw, J. (2019). A library of proton-transfer reactions of H_3O^+ ions used for trace gas detection. *Journal of the American Society for Mass Spectrometry*, *30*(7), 1330–1335. https://doi.org/10.1007/s13361-019-02209-3

Palm, B. B., Liu, X., Jimenez, J. L., & Thornton, J. A. (2019). Performance of a new coaxial ion-molecule reaction region for low-pressure chemical ionization mass spectrometry with reduced instrument wall interactions. *Atmospheric Measurement Techniques*, *12*(11), 5829–5844. https://doi.org/10.5194/amt-12-5829-2019

Pan, X., Ichoku, C., Chin, M., Bian, H., Darmenov, A., Colarco, P., et al. (2020). Six global biomass burning emission datasets: Intercomparison and application in one global aerosol model. *Atmospheric Chemistry and Physics*, *20*(2), 969–994. https://doi.org/10.5194/acp-20-969-2020

Peng, Q., Palm, B. B., Melander, K. E., Lee, B. H., Hall, S. R., Ullmann, K., et al. (2020). HONO emissions from western U.S. wildfires provide dominant radical source in fresh wildfire smoke. *Environmental Science & Technology*, *54*(10), 5954–5963. https://doi.org/10.1021/acs.est.0c00126

Pommier, M., Clerbaux, C., & Coheur, P.-F. (2017). Determination of enhancement ratios of HCOOH relative to CO in biomass burning plumes by the Infrared Atmospheric Sounding Interferometer (IASI). *Atmospheric Chemistry and Physics*, *17*(18), 11089–11105. https://doi.org/10.5194/acp-17-11089-2017

Prichard, S. J., O'Neill, S. M., Eagle, P., Andreu, A. G., Drye, B., Dubowy, J., et al. (2020). Wildland fire emission factors in North America: Synthesis of existing data, measurement needs and management applications. *International Journal of Wildland Fire*, *29*(2), 132. https://doi.org/10.1071/WF19066

R Core Team. (2019). *R: A language and environment for statistical computing*. R Foundation for Statistical Computing. Retrieved from https://www.R-project.org/

Roberts, J. M., Stockwell, C. E., Yokelson, R. J., de Gouw, J., Liu, Y., Selimovic, V., et al. (2020). The nitrogen budget of laboratory-simulated western US wildfires during the FIREX 2016 Fire Lab study. *Atmospheric Chemistry and Physics*, *20*(14), 8807–8826. https://doi.org/10.5194/acp-20-8807-2020

RStudio Team. (2020). *RStudio: Integrated development environment for R*. RStudio, PBC. Retrieved from http://www.rstudio.com/

Russo, R. S., Zhou, Y., White, M. L., Mao, H., Talbot, R., & Sive, B. C. (2010). Multi-year (2004-2008) record of nonmethane hydrocarbons and halocarbons in New England: Seasonal variations and regional sources. *Atmospheric Chemistry and Physics*, *10*(10), 4909–4929. https://doi.org/10.5194/acp-10-4909-2010

Santín, C., Doerr, S. H., Preston, C. M., & González-Rodríguez, G. (2015). Pyrogenic organic matter production from wildfires: A missing sink in the global carbon cycle. *Global Change Biology*, *21*(4), 1621–1633. https://doi.org/10.1111/gcb.12800

Schwarz, J. P., Gao, R. S., Spackman, J. R., Watts, L. A., Thomson, D. S., Fahey, D. W., et al. (2008). Measurement of the mixing state, mass, and optical size of individual black carbon particles in urban and biomass burning emissions. *Geophysical Research Letters*, *35*(13). https://doi.org/10.1029/2008GL033968

Sekimoto, K., Koss, A. R., Gilman, J. B., Selimovic, V., Coggon, M. M., Zarzana, K. J., et al. (2018). High- and low-temperature pyrolysis profiles describe volatile organic compound emissions from western US wildfire fuels. *Atmospheric Chemistry and Physics*, *18*(13), 9263–9281. https://doi.org/10.5194/acp-18-9263-2018

Sekimoto, K., Li, S.-M., Yuan, B., Koss, A., Coggon, M., Warneke, C., & de Gouw, J. (2017). Calculation of the sensitivity of proton-transfer-reaction mass spectrometry (PTR-MS) for organic trace gases using molecular properties. *International Journal of Mass Spectrometry*, *421*, 71–94. https://doi.org/10.1016/j.ijms.2017.04.006

Selimovic, V., Yokelson, R. J., McMeeking, G. R., & Coefield, S. (2019). In situ measurements of trace gases, PM, and aerosol optical properties during the 2017 NW US wildfire smoke event. *Atmospheric Chemistry and Physics*, *19*(6), 3905–3926. https://doi.org/10.5194/acp-19-3905-2019

Selimovic, V., Yokelson, R. J., Warneke, C., Roberts, J. M., de Gouw, J., Reardon, J., & Griffith, D. W. T. (2018). Aerosol optical properties and trace gas emissions by PAX and OP-FTIR for laboratory-simulated western US wildfires during FIREX. *Atmospheric Chemistry and Physics*, *18*(4), 2929–2948. https://doi.org/10.5194/acp-18-2929-2018

Stockwell, C. E., Veres, P. R., Williams, J., & Yokelson, R. J. (2015). Characterization of biomass burning emissions from cooking fires, peat, crop residue, and other fuels with high-resolution proton-transfer-reaction time-of-flight mass spectrometry. *Atmospheric Chemistry and Physics*, *15*(2), 845–865. https://doi.org/10.5194/acp-15-845-2015

Stockwell, C. E., Yokelson, R. J., Kreidenweis, S. M., Robinson, A. L., DeMott, P. J., Sullivan, R. C., et al. (2014). Trace gas emissions from combustion of peat, crop residue, domestic biofuels, grasses, and other fuels: Configuration and Fourier transform infrared (FTIR) component of the fourth Fire Lab at Missoula Experiment (FLAME-4). *Atmospheric Chemistry and Physics*, *14*(18), 9727–9754. https://doi.org/10.5194/acp-14-9727-2014

Urbanski, S. (2014). Wildland fire emissions, carbon, and climate: Emission factors. *Forest Ecology and Management*, *317*, 51–60. https://doi.org/10.1016/j.foreco.2013.05.045

U.S. Environmental Protection Agency. (2020). *2017 National Emissions Inventory (NEI) Technical Support Document (TSD)*. Retrieved from https://www.epa.gov/sites/production/files/2020-04/documents/nei2017_tsd_full_30apr2020.pdf

van der Werf, G. R., Randerson, J. T., Giglio, L., van Leeuwen, T. T., Chen, Y., Rogers, B. M., et al. (2017). Global fire emissions estimates during 1997-2016. *Earth System Science Data*, *9*(2), 697–720. https://doi.org/10.5194/essd-9-697-2017

Veres, P., Gilman, J. B., Roberts, J. M., Kuster, W. C., Warneke, C., Burling, I. R., & de Gouw, J. (2010). Development and validation of a portable gas phase standard generation and calibration system for volatile organic compounds. *Atmospheric Measurement Techniques*, *3*(3), 683–691. https://doi.org/10.5194/amt-3-683-2010

Vlasenko, A., Macdonald, A. M., Sjostedt, S. J., & Abbatt, J. P. D. (2010). Formaldehyde measurements by Proton transfer reaction – Mass Spectrometry (PTR-MS): Correction for humidity effects. *Atmospheric Measurement Techniques*, *3*(4), 1055–1062. https://doi.org/10.5194/amt-3-1055-2010

Warneke, C., Veres, P., Holloway, J. S., Stutz, J., Tsai, C., Alvarez, S., et al. (2011). Airborne formaldehyde measurements using PTR-MS: Calibration, humidity dependence, inter-comparison and initial results. *Atmospheric Measurement Techniques*, *4*(10), 2345–2358. https://doi.org/10.5194/amt-4-2345-2011

Westerling, A. L. (2006). Warming and earlier spring increase western U.S. forest wildfire activity. *Science*, *313*(5789), 940–943. https://doi.org/10.1126/science.1128834

Westerling, A. L. (2016). Increasing western US forest wildfire activity: Sensitivity to changes in the timing of spring. *Philosophical Transactions of the Royal Society B*, *371*(1696), 20150178. https://doi.org/10.1098/rstb.2015.0178

Wickham, H. (2016). *ggplot2: Elegant graphics for data analysis*. Springer-Verlag New York. Retrieved from https://ggplot2.tidyverse.org

Wickham, H., François, R., Henry, L., & Müller, K. (2019). *Dplyr: A grammar of data manipulation*.

Yokelson, R. J., Burling, I. R., Gilman, J. B., Warneke, C., Stockwell, C. E., de Gouw, J., et al. (2013). Coupling field and laboratory measurements to estimate the emission factors of identified and unidentified trace gases for prescribed fires. *Atmospheric Chemistry and Physics*, *13*(1), 89–116. https://doi.org/10.5194/acp-13-89-2013

Yokelson, R. J., Christian, T. J., Karl, T. G., & Guenther, A. (2008). The tropical forest and fire emissions experiment: laboratory fire measurements and synthesis of campaign data. *Atmospheric Chemistry and Physics*, *8*(13), 3509–3527. https://doi.org/10.5194/acp-8-3509-2008

Yokelson, R. J., Crounse, J. D., DeCarlo, P. F., Karl, T., Urbanski, S., Atlas, E., et al. (2009). Emissions from biomass burning in the Yucatan. *Atmospheric Chemistry and Physics*, *9*(15), 5785–5812. https://doi.org/10.5194/acp-9-5785-2009

Yokelson, R. J., Goode, J. G., Ward, D. E., Susott, R. A., Babbitt, R. E., Wade, D. D., et al. (1999). Emissions of formaldehyde, acetic acid, methanol, and other trace gases from biomass fires in North Carolina measured by airborne Fourier transform infrared spectroscopy. *Journal of Geophysical Research*, *104*(D23), 30109–30125. https://doi.org/10.1029/1999JD900817

Yokelson, R. J., Griffith, D. W. T., & Ward, D. E. (1996). Open-path Fourier transform infrared studies of large-scale laboratory biomass fires. *Journal of Geophysical Research*, *101*(D15), 21067–21080. https://doi.org/10.1029/96JD01800

Yuan, B., Koss, A. R., Warneke, C., Coggon, M., Sekimoto, K., & de Gouw, J. A. (2017). Proton-transfer-reaction mass spectrometry: Applications in atmospheric sciences. *Chemical Reviews*, *117*(21), 13187–13229. https://doi.org/10.1021/acs.chemrev.7b00325

Yuan, B., Warneke, C., Shao, M., & de Gouw, J. A. (2014). Interpretation of volatile organic compound measurements by proton-transfer-reaction mass spectrometry over the deepwater horizon oil spill. *International Journal of Mass Spectrometry*, *358*, 43–48. https://doi.org/10.1016/j.ijms.2013.11.006

Zhang, F., Wang, J., Ichoku, C., Hyer, E. J., Yang, Z., Ge, C., et al. (2014). Sensitivity of mesoscale modeling of smoke direct radiative effect to the emission inventory: A case study in northern sub-Saharan African region. *Environmental Research Letters*, *9*(7), 075002. https://doi.org/10.1088/1748-9326/9/7/075002

Zhou, Y., Shively, D., Mao, H., Russo, R. S., Pape, B., Mower, R. N., et al. (2010). Air toxic emissions from snowmobiles in Yellowstone National Park. *Environmental Science & Technology*, *44*(1), 222–228. https://doi.org/10.1021/es9018578